J. Fluid Mech. (1990), *vol.* 221, *pp.* 311–347
Printed in Great Britain

Non-parallel stability of a flat-plate boundary layer using the complete Navier–Stokes equations

By H. FASEL† AND U. KONZELMANN
Institut A für Mechanik, Universität Stuttgart, Stuttgart, FRG

(Received 10 July 1989 and in revised form 1 May 1990)

Non-parallel effects which are due to the growing boundary layer are investigated by direct numerical integration of the complete Navier–Stokes equations for incompressible flows. The problem formulation is spatial, i.e. disturbances may grow or decay in the downstream direction as in the physical experiments. In the past various non-parallel theories were published that differ considerably from each other in both approach and interpretation of the results. In this paper a detailed comparison of the Navier–Stokes calculation with the various non-parallel theories is provided. It is shown, that the good agreement of some of the theories with experiments is fortuitous and that the difference between experiments and theories concerning the branch I neutral location cannot be explained by non-parallel effects.

1. Introduction

For a disturbance environment with very small amplitudes, the first stage of the transition process in a flat-plate boundary layer is governed by the amplification of two-dimensional disturbances. The development during this first stage, in particular the growth or decay of the so-called Tollmien–Schlichting waves is well described by the linear stability theory (Heisenberg 1924; Tollmien 1929; Schlichting 1933). Historically, in this stability theory the temporal approach was considered first: for this, the growth or decay of the disturbances was assumed to be in time direction. However, in the pioneering experiments by Schubauer & Skramstad (1947) it was clearly shown that the disturbance development was in the downstream direction, with amplitudes of the disturbances growing or decaying with increasing distance from the leading edge. Schubauer & Skramstad used the phase velocity of the disturbance waves for comparing measurement with theory. Gaster (1962) has shown, however, that the use of the phase velocity for relating the temporal development of the theory with the spatial development of the experiments, as done by Schubauer & Skramstad, was only approximately correct. Thereupon, as suggested by Gaster (1965), the stability problem was reformulated into a 'spatial' approach (see for example Jordinson 1970) which allowed a direct comparison of theory and experiment.

Nevertheless, qualitative and quantitative differences between the spatial theory and experiments remained. The discrepancies were attributed to the so-called non-parallel effects which were excluded in the standard quasi-parallel theory (Jordinson 1970). In this theory it was argued that owing to the slow growth of the boundary

† On sabbatical leave from the University of Arizona, Aerospace and Mechanical Engineering Department, Tucson, AZ 85721, USA.

layer, the assumptions of a parallel base flow $U = U(y)$, $V = 0$ and of a disturbance amplitude distribution that is only dependent on the normal coordinate y (and not on the downstream coordinate x) would be justified. With these assumptions the governing equations (linearized Navier–Stokes equations for the disturbance flow) became separable and lead to an ordinary differential equation, the Orr–Sommerfeld equation, that is amenable to numerical solutions. However, at that time it was not obvious what consequences the parallel assumption would have. When the parallel theory did not fully agree with the experimental measurements (in particular with respect to the growth rates and the critical Reynolds number) the parallel assumption was suspected to be responsible. Consequently, efforts were made to remedy the situation by attempting to include the non-parallel effects resulting from the boundary-layer growth in the downstream direction.

The efforts to predict the amplification behaviour of the disturbances more accurately were not only driven by academic motives. Rather, the demands of engineering design required a more accurate prediction of the transition location. For example, the most commonly used methods for transition prediction (e^N methods, by Smith & Gamberoni 1956; Van Ingen 1956), require accurate numbers for the growth rates of the two-dimensional waves. Further, in modern efforts of transition control by both passive (such as heating/cooling, suction/blowing) or active control (wave cancellation by feedback control, see Liepmann, Brown & Nosenchuck 1982; Liepmann & Nosenchuck 1982) an accurate account concerning the efficiency of these measures can only be made if the effects of the non-parallel base flow are understood.

One of the first attempts to account for the non-parallel effects was by Barry & Ross (1970) who allowed $V \neq 0$ and included some of the streamwise derivatives of the base flow so that the governing equations still remained separable. These corrections lead to an only slightly better agreement with the experiments (Ross *et al.* 1970; Schubauer & Skramstad 1947) as the unstable region became only moderately enlarged. In particular, the critical Reynolds number (based on the displacement thickness) decreased to $Re_{\text{crit}} = 500$ from $Re_{\text{crit}} = 520$ for the parallel theory. Other attempts based on expansion procedures (for example by Lanchon & Eckhaus 1964; Volodin 1973; Ling & Reynolds 1973) were also not successful in explaining the discrepancies between experiments and theory.

On the other hand, upon publication of two papers by Bouthier (1972, 1973) the discrepancy appeared to be resolved at first as the neutral loop obtained from his analysis matched the experimental neutral points of both Schubauer & Skramstad and Ross *et al.* In his analysis Bouthier applied the method of multiple scales to separate out the small parameter that controlled the distortion of the coordinates from the viscous terms in the governing equation.

However, a closer examination of Bouthier's analysis and the results obtained with it revealed that the agreement was rather fortuitous. Bouthier introduced the concept of 'partial' and 'total' instability. In judging stability or instability Bouthier measured the streamwise decay or growth of the local kinetic energy $e = \overline{u'}^2 + \overline{v'}^2$ (overbar denotes the time average over one period). For total instability the kinetic energy increases at all η values ($\eta = y[U_\infty/(2x\nu)]^{\frac{1}{2}}$), boundary layer similarity coordinate) when following the disturbance on trajectories $\eta = \text{constant}$ in the downstream direction. For partial instability, following along constant η, the kinetic energy increases for at least one η location while decreasing at other η locations. When comparing his results with experiments, Bouthier used the neutral points from his analysis that, based on his partial stability concept, resulted in the lowest possible

Reynolds number for branch I and resulted in the highest possible Reynolds number for branch II of the neutral stability curve. This interpretation lead to a considerably increased instability region with a critical Reynolds number of approximately $Re_{\text{crit}} = 350$ and consequently lead to a much better agreement with the experiments. However, this comparison with the experiments is not a proper one because (*a*) the experimental measurements were for the u' disturbance and not for the kinetic energy and (*b*) the experimental neutral points were obtained by following the u' disturbances either at a constant distance from the wall (Schubauer & Skramstad) or at a constant η as in Ross *et al.*

In a fundamental study on non-parallel effects, Gaster (1974) has clearly shown that stability characteristics and thus the locations of the neutral points depend strongly on the criteria used. Therefore, when comparing theoretical results with experimental measurements or numerical simulations it is essential that identical criteria are used for defining instability. Gaster used an analysis different from previous attempts. His analysis is in a sense more direct although an iteration scheme is employed to develop a series. For this, the parallel flow approximation serves as a suitable trial solution and successive correction terms lead to a series in descending powers of $Re^{\frac{1}{2}}$.

With this non-parallel theory Gaster has investigated the effect of different criteria (such as the kinetic energy integral

$$E = \int_0^\infty (\bar{u}'^2 + \bar{v}'^2)\,\mathrm{d}y \quad \text{or} \quad E_\eta = \int_0^\infty \bar{u}'^2 \mathrm{d}\eta,$$

inner (first) and outer (second) maximum of u') on the stability characteristics and in particular also on the neutral curve. Gaster clearly demonstrated that different criteria can affect the neutral curve and thus the critical Reynolds number. However, none of the criteria that he considered lead to the neutral loops and low critical Reynolds number that were obtained by Bouthier. In particular, in a proper comparison with the experiments, i.e. using the same criteria for judging stability as in the experiments, the neutral curves of Gaster's theory do not coincide as closely with the experimental points of Schubauer & Skramstad nor with those of Ross *et al.* Although the non-parallel effects obtained by Gaster reduced the critical Reynolds number from 520 (for parallel theory) to about 480, the deviation from the experimental critical Reynolds number obtained by Ross *et al.* of approximately 400 still remained significant.

Based on a non-parallel analysis using multiple scales Saric & Nayfeh (1975) calculated a correction for the eigenvalues which lead to non-parallel growth rates that represented a markedly bigger deviation from the parallel results than those obtained by Gaster. Especially, the neutral loop enclosed a much larger unstable region and appeared to match the experimental data remarkably well, in particular also for branch I and the high frequencies (see figure 1 of Saric & Nayfeh 1975). The critical Reynolds number obtained was about 400, as that of Ross *et al.* However, this paper did not address the issue of how different criteria may affect the results. This question was discussed in a later paper (Saric & Nayfeh 1977) and it was mentioned that the neutral curve given in the earlier paper (Saric & Nayfeh 1975) would relate to the first maximum of the u'-disturbance.

Smith (1979) investigated non-parallel effects by using the triple-deck theory. In his analysis the parallel-flow solution is the leading term and the non-parallel effects emerge from the asymptotic expansions. Although the theory is strictly valid for large Reynolds numbers only, comparison was also made for smaller Reynolds

numbers. In general, the non-parallel effects appear to be stronger than in the analysis by Gaster (1974). However, as stated by Smith, his analysis should yield results identical to those of the theory by Gaster if in both approaches infinitely many terms were used.

Another non-parallel analysis by Van Stijn & Van de Vooren (1983) using an approach different from both Gaster and Saric & Nayfeh yielded results very close to those by Gaster, thus supporting Gaster's analysis. More recently, an analysis by Bridges & Morris (1987) which is similar to that of Saric & Nayfeh (1975) yielded non-parallel effects that at first sight appear to be somewhat stronger (based on a neutral curve given in the paper) than those of Gaster, although no direct comparison was presented with either Gaster or Saric & Nayfeh.

In summary, to date a number of non-parallel analyses have been presented which yield results that in some instances match the experimental data very well but at the same time disagree with other non-parallel theories. The discrepancies may be due to deficiencies in the theoretical models as in all analyses certain terms had to be neglected to keep the problem separable. Therefore, in all these analyses the non-parallel effects could only be considered approximately. Thus, differences between the theories may be due to the different judgement by the authors of which terms are relevant and have to be kept, and which are not and could be safely neglected. In addition, differences may be due to the different interpretation and the true meaning of the results.

Because of this somewhat confusing picture, with the present study an attempt was made to investigate non-parallel stability effects based on a model that includes all possible effects. Therefore, no bias is introduced as to which terms are relevant and which are not. The present study is based on the complete Navier–Stokes equations. However, since no assumptions concerning the base flow are made, the problem remains unseparable and does not reduce to ordinary differential equations.

Therefore, the Navier–Stokes equations for two-dimensional, incompressible flows are solved directly using an accurate numerical procedure. This approach in a sense represents a direct numerical simulation of the laboratory experiments by Schubauer & Skramstad or Ross *et al.*, as well as others, where the response of the boundary layer to a local wavemaker (for example, a vibrating ribbon) subjected to different frequencies was investigated. In particular, our model is a spatial one which allowed direct calculation of the spatial downstream development of the disturbance waves as observed in the laboratory experiments.

Thus, our calculations allow direct and detailed comparison of the results with the measurements in experiments on one hand and with results from the various non-parallel theories on the other. These calculations should help to shed light on the discrepancies between the various non-parallel theories and between the theories and experiments.

In this paper, after a brief discussion of the numerical model which is based on the complete Navier–Stokes equations, relevant results of our calculations are presented and are compared in detail with results from non-parallel theories and experimental measurements.

2. Numerical model

In this paper, the effects of the boundary-layer growth on the stability ('non-parallel effects') are investigated by direct numerical simulations based on the complete Navier–Stokes equations. The numerical model is similar to the one used

in Fasel (1974, 1976). In particular, the model is a spatial one, thus allowing a spatially growing boundary layer, and allowing the amplification of the disturbances in the downstream direction. All possible non-parallel effects are included in this model. In fact, in this model the nonlinear effects are included also. However, for the results presented in this paper the nonlinear effects are negligible owing to the extremely small disturbance amplitudes used in these calculations.

2.1. *Governing equations*

In the present investigations, the Navier–Stokes equations for two-dimensional incompressible flows are used in a vorticity–velocity formulation with the vorticity transport equation

$$\frac{\partial \omega}{\partial t}+u\frac{\partial \omega}{\partial x}+v\frac{\partial \omega}{\partial y}=\nabla^2\omega, \tag{2.1}$$

and two Poisson equations for the two velocity components u and v in the x- and y-direction, respectively

$$\nabla^2 u=\frac{\partial \omega}{\partial y}, \tag{2.2}$$

$$\nabla^2 v=-\frac{\partial \omega}{\partial x}. \tag{2.3}$$

The Poisson equations result from the definition of vorticity

$$\omega=\frac{\partial u}{\partial y}-\frac{1}{Re}\frac{\partial v}{\partial x}, \tag{2.4}$$

and the continuity equation

$$\frac{\partial u}{\partial x}+\frac{\partial v}{\partial y}=0. \tag{2.5}$$

Equations (2.1)–(2.5) are dimensionless. The dimensionless quantities relate to the corresponding dimensional ones, denoted by overbars, as follows:

$$\omega=\frac{\bar{\omega}\bar{L}}{\bar{U}_\infty (Re)^{\frac{1}{2}}}, \quad u=\frac{\bar{u}}{\bar{U}_\infty}, \quad v=\frac{\bar{v}}{\bar{U}_\infty}(Re)^{\frac{1}{2}},$$

$$x=\frac{\bar{x}-\bar{x}_0}{\bar{L}}, \quad y=\frac{\bar{y}}{\bar{L}}(Re)^{\frac{1}{2}}, \quad t=\bar{t}\,\frac{\bar{U}_\infty}{L}.$$

$\bar{U}_\infty$ is the freestream velocity, $\bar{L}$ is a reference length, $\bar{x}_0$ the distance from the leading edge (see figure 1) and Re is a Reynolds number defined as $Re=\bar{U}_\infty \bar{L}/\bar{\nu}$ where $\bar{\nu}$ is the kinematic viscosity. The Laplace operator ∇^2 in equations (2.1)–(2.3) is then given by

$$\nabla^2=\frac{1}{Re}\frac{\partial^2}{\partial x^2}+\frac{\partial^2}{\partial y^2}.$$

The governing equations (2.1)–(2.3) are solved numerically in a rectangular domain shown schematically in figure 1. A set of boundary conditions and initial conditions is required for the solution of this system of equations.

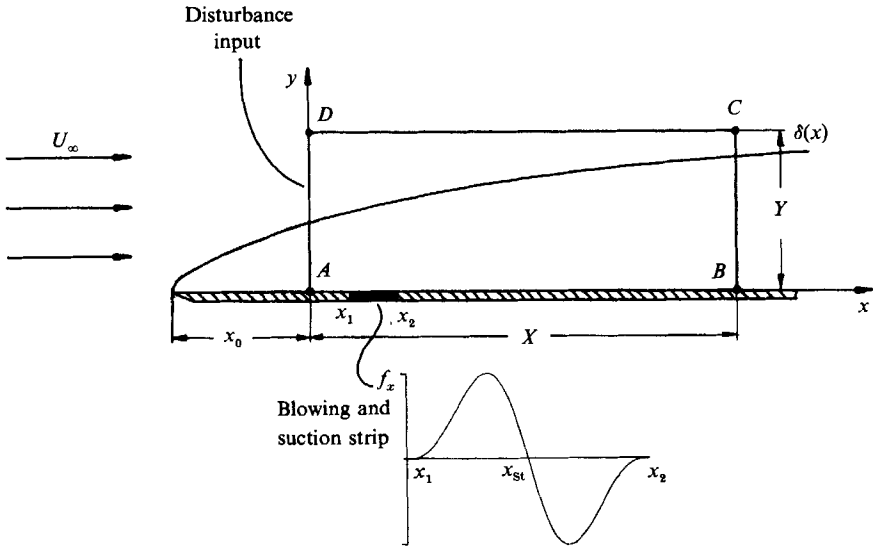

FIGURE 1. Integration domain.

2.2. *Boundary and initial conditions*

The specification of proper boundary conditions and their implementation into the numerical method is an issue of great complexity for the problem at hand. The concerns and difficulties in association with such direct numerical simulations were discussed earlier in great detail (see Fasel 1974, 1976, 1979) and will, therefore, not be repeated here. Rather, we will only summarize the set of boundary conditions which was selected and used for the present study.

For the calculation of the unsteady disturbed flow an initial condition is required. For this the flow variables are specified in the entire integration domain for an initial time t_0

$$\left.\begin{aligned} u(x,y,t_0) &= U(x,y), \\ v(x,y,t_0) &= V(x,y), \\ \omega(x,y,t_0) &= \Omega(x,y), \end{aligned}\right\} \tag{2.6}$$

where the initial flow field U, V, Ω is obtained from the numerical solution of the Navier–Stokes equations (2.1)–(2.3) for the steady boundary-layer flow, that is, without the term $\partial\omega/\partial t$ in equation (2.1). Thus, with such an initial condition, the flow is initially undisturbed and the disturbances are then introduced during the unsteady cycle of the computation.

At the inflow boundary A–D at $x = 0$ Blasius profiles (index Bl) are specified for the calculation of the steady flow

$$U(0,y) = u_{\mathrm{Bl}}(0,y), \quad V(0,y) = v_{\mathrm{Bl}}(0,y), \quad \Omega(0,y) = \omega_{\mathrm{Bl}}(0,y). \tag{2.7}$$

For the unsteady calculation at A–D, time-periodic perturbations can be superimposed onto the Blasius profiles:

$$\left.\begin{aligned} u(0,y,t) &= u_{\mathrm{Bl}}(0,y)+u_{\mathrm{p}}(y,t), \\ v(0,y,t) &= v_{\mathrm{Bl}}(0,y)+v_{\mathrm{p}}(y,t), \\ \omega(0,y,t) &= \omega_{\mathrm{Bl}}(0,y)+\omega_{\mathrm{p}}(y,t). \end{aligned}\right\} \tag{2.8}$$

The perturbation functions u_p, v_p, ω_p are obtained from the eigensolutions of the Orr–Sommerfeld equation, where non-parallel effects on the eigenfunctions are neglected. As will be shown later, non-parallel effects on the eigenfunctions are very small and can therefore be justifiably neglected for this disturbance generation. With this, realistic Tollmien–Schlichting-type disturbances can be generated which propagate downstream and are amplified or damped in the downstream direction depending on the local Reynolds number. Thus, the disturbance behaviour is as in the laboratory experiments when the disturbance wave is generated by a local wavemaker, such as a vibrating ribbon (Schubauer & Skramstad; Ross *et al.*; Kachanov, Kozlov & Levchenko 1979) or a heater strip (Liepmann *et al.* 1982).

An alternative method also used here to generate the disturbances is by periodic blowing and suction through a narrow strip at the wall as discussed in connection with the boundary conditions at the wall.

Along the wall on boundary A–B the boundary conditions for the steady flow are

$$\left.\begin{aligned} U(x,0) = 0, \quad V(x,0) = 0, \\ \frac{\partial \Omega(x,0)}{\partial x} = -\frac{\partial^2 V(x,0)}{\partial y^2}, \end{aligned}\right\} \tag{2.9}$$

and for the unsteady flow

$$\left.\begin{aligned} u(x,0,t) = 0, \quad v(x,0,t) = f(x,t), \\ \frac{\partial \omega(x,0,t)}{\partial x} = -\frac{\partial^2 v(x,0,t)}{\partial y^2} - \frac{1}{Re}\frac{\partial^2 f(x,t)}{\partial x^2}. \end{aligned}\right\} \tag{2.10}$$

The condition for the vorticity is obtained from the Poisson equations (2.3) for the v-velocity component.

Thus, at the wall we have no slip but we assume a permeable wall to allow for a time-dependent localized blowing and suction when the alternative method is used to generate Tollmien–Schlichting waves as mentioned before. For example, for the results presented in this paper we used $f(x,t) = f_x(x)\sin(\beta t)$, where β is the disturbance frequency and for f_x

$$f_x = 15.1875\,\xi^5 - 35.4375\,\xi^4 + 20.25\,\xi^3 \tag{2.11}$$

was used (see figure 1), with

$$\xi = \frac{x - x_1}{x_{st} - x_1} \quad \text{for} \quad x_1 < x < x_{st},$$

and

$$\xi = \frac{x_2 - x}{x_2 - x_{st}} \quad \text{for} \quad x_{st} < x < x_2.$$

This distribution produced clean localized vorticity disturbances and caused negligible time-dependent changes of the mean flow. Detailed comparison with calculations where the disturbances were introduced through the inflow boundary has shown that with disturbances generated by localized blowing and suction (Konzelmann, Rist & Fasel 1987) the downstream development is the same as with the disturbances generated at the inflow boundary except near the blowing and suction strip. The disturbance generation at the inflow boundary using (2.8),

however, allows for a shorter x-integration domain because the local generation of the waves by a localized wavemaker requires additional integration domain and adequate local numerical resolution. On the other hand, the disturbance generation employing the blowing and suction strip represents a more realistic situation, and is also applicable for large-amplitude calculations (not considered here) for which the use of linear eigenfunctions at the inflow boundary is not justified.

At the outflow boundary B–C we use, for the steady flow calculations,

$$\frac{\partial^2 U(X,y)}{\partial x^2}=0, \quad \frac{\partial^2 V(X,y)}{\partial x^2}=0, \quad \frac{\partial^2 \Omega(X,y)}{\partial x^2}=0, \tag{2.12}$$

and for the unsteady flow calculations,

$$\left.\begin{aligned} \frac{\partial^2 u(X,y)}{\partial x^2} &= -\alpha^2 u'(X,y), \\ \frac{\partial^2 v(X,y)}{dx^2} &= -\alpha^2 v'(X,y), \\ \frac{\partial^2 \omega(X,y)}{\partial x^2} &= -\alpha^2 \omega'(X,y), \end{aligned}\right\} \tag{2.13}$$

where the prime denotes the disturbance variables

$$u'=U-u, \quad v'=V-v, \quad \omega'=\Omega-\omega, \tag{2.14}$$

where α is the local wavenumber of the disturbance waves, $\alpha=2\pi/\lambda$ (λ is the wavelength). The values for α can be taken from either the local solution of the Orr–Sommerfeld equation where a correction could be made for the non-parallel effects on the wavenumber. Or, α could be determined iteratively as suggested in Fasel (1974, 1979). However, for the present investigations values for α were simply taken from the local Orr–Sommerfeld solution without non-parallel correction. Numerous test calculations have shown that for small amplitudes the upstream effect of these outflow conditions was relatively small even if very approximate values for α were used. For example, for α values differing up to $\pm 50\,\%$ from the Orr–Sommerfeld values, the Navier–Stokes solution was practically not affected for more than one wavelength upstream of the outflow boundary. In summary, boundary conditions (2.13) in combination with governing equations (2.1)–(2.3) allow for smooth propagation of small-amplitude waves through the outflow boundary, where the strong insensitivity of the Navier–Stokes results with regard to variations of α in these boundary conditions was of particular advantage.

The free-stream boundary C–D is assumed to be far enough from the wall (typically six to fourteen displacement thicknesses) so that the assumption of an inviscid flow is justified. Therefore, for the steady calculation we are using the boundary conditions

$$\left.\begin{aligned} U(x,Y) &= 1, \\ \frac{\partial V(x,Y)}{\partial y} &= 0, \\ \Omega(x,Y) &= 0. \end{aligned}\right\} \tag{2.15}$$

For the calculation of the unsteady flow the disturbance velocity components are assumed to decay exponentially while the vorticity vanishes:

$$\left.\begin{aligned} \frac{\partial u'(x,Y)}{\partial y} &= -\frac{\alpha}{(Re)^{\frac{1}{2}}}u'(x,Y), \\ \frac{\partial v'(x,Y)}{\partial y} &= -\frac{\alpha}{(Re)^{\frac{1}{2}}}v'(x,Y), \\ \omega(x,Y) &= 0. \end{aligned}\right\} \tag{2.16}$$

As for the outflow conditions (2.13), for the present calculations the values for α in (2.16) were also taken from the Orr–Sommerfeld solution without a non-parallel correction. Test calculations have shown that deviations of α due to non-parallel corrections would have been too small to affect the numerical Navier–Stokes solutions within the integration domain when the free-stream boundary was sufficiently far away from the flat plate (for the present calculations $Y \approx 6\delta_1$ at the outflow boundary). As seen later from the results (figure 4) $\omega = 0$ at the free-stream boundary is well justified. However, analogous conditions for u' and v' (i.e. $u' = 0$, $v' = 0$) would not be appropriate. u' and v' decay rather slowly in the y-direction and therefore a rather large domain in y would be required if $u' = 0$, $v' = 0$ were to be used. Therefore, use of the conditions (2.16) allows a much smaller y-domain and thus considerable savings in computer memory and computer time. Another possible option, namely that of a coordinate transformation in the y-direction such that a domain from $y = 0$ to $y = \infty$ would be mapped onto a finite domain, say from 0 to 1, was rejected for this study. Although this would allow the use of Dirichlet conditions $u' = 0$ and $v' = 0$ at $y = \infty$, difficulties arise when a finite-difference method is used (as in the present study, see §2.3). With such a transformation, a so-called artificial viscosity (see Roache 1982) may be introduced, which of course may affect the numerical results and may therefore render the detailed quantitative comparison somewhat ambiguous.

2.3. *Numerical method*

The governing equations (2.1)–(2.3) together with the boundary conditions specified in §2.2 are solved numerically using a finite-difference method. The method is based on the fully implicit difference method with second-order accuracy in time and in the x- and y-direction (Fasel 1976). However, for the present study the accuracy in the spatial coordinates x and y was increased from second to fourth order as discussed in Bestek (1980). The considerably higher accuracy allows much more accurate computations and/or lower computation times, because of the larger grid sizes that can be used for equal accuracy when compared to an analogous calculation with second-order accuracy. Since one of the major objectives of the present study is a detailed, reliable comparison with various non-parallel theories, emphasis here is clearly on accuracy.

The difference equations resulting from the fully implicit method are solved using a coupled line iteration procedure as discussed in Fasel (1974) and Bestek (1980).

3. Numerical results

Results of a number of calculations are presented. The calculation cases were selected to allow comparison with the results of various non-parallel theories and/or experimental measurements. Owing to the limited space for discussion, the

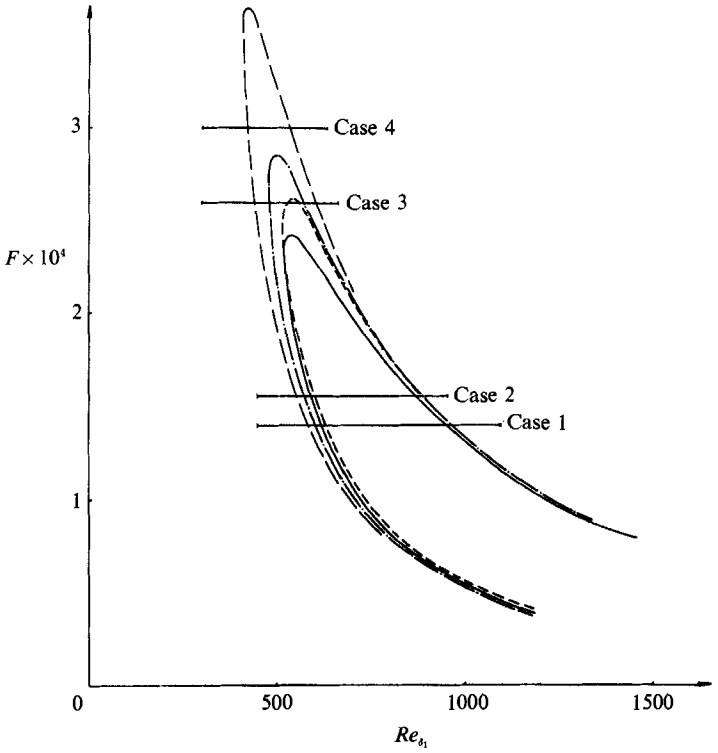

FIGURE 2. Stability diagram of linear stability theory with ——, the neutral curve of the parallel theory and various neutral curves of non-parallel theories: – – –, inner maximum u' (Gaster 1974); —·—, kinetic energy integral E (Gaster 1974); ——, inner maximum u' (Saric & Nayfeh 1975). The Navier–Stokes calculations discussed in this paper are indicated by the horizontal bars.

calculations were selected on their possible merit to either lend support to the various theories or to help explain certain discrepancies. In particular, calculations were performed to allow comparison with the results of linear stability theory calculations (parallel theory) by Jordinson, of the non-parallel theories by Bouthier (1972, 1973), Gaster (1974), Saric & Nayfeh (1975, 1977), Van Stijn & Van de Vooren (1983), Bridges & Morris (1987), and of the experiments of Ross *et al.* (1970) as well as Kachanov *et al.* (1979).

The calculation cases which will be discussed are identified in figure 2. In this stability diagram of dimensionless frequency parameter F (defined as $F = \bar{\beta}\bar{\nu}/\bar{U}_\infty^2$; $\bar{\beta}$ is the dimensional frequency) versus the Reynolds number based on the displacement thickness, $Re_{\delta_1} = \bar{U}_\infty \bar{\delta}_1/\bar{\nu}$, neutral stability curves of several non-parallel theories are displayed.

The neutral loops as obtained by Gaster (1974) are based on two different stability criteria, namely for the kinetic energy integral E and for the inner maximum of u'. (The labelling for the neutral curves given in figure 2 of Gaster (1974) for the inner and outer maximum of u' are reversed; Gaster 1983, private communication). Further, the neutral loop by Saric & Nayfeh is displayed. For comparison the neutral curves obtained from standard parallel theory is given also. It is obvious that considerable deviations exist between the various non-parallel results, especially for the higher frequencies and for branch I and thus also for the critical Reynolds number.

Case	F	Dist.	Δx	Δy	Δt	x_0	$Re_{\delta_1}(x_0)$	X	Y
1	1.4×10^{-4}	*a*	0.0133	0.2511	0.0112	0.6839	450	3.378	17.07
		b	0.0138	0.2724	0.00345	0.5403	400	3.588	17.71
2	1.56×10^{-4}	*a*	0.0120	0.2302	0.0101	0.6839	450	2.400	15.65
3	2.6×10^{-4}	*a*	0.0078	0.1674	0.0060	0.3039	300	1.186	11.38
		b	0.0063	0.1660	0.00151	0.3039	300	1.26	13.28
4	3.0×10^{-4}	*a*	0.0069	0.1674	0.0052	0.3039	300	1.049	11.38
		b	0.0063	0.1660	0.00131	0.3039	300	1.260	13.28

TABLE 1. Summary of parameters used for the four calculations cases. *a*, Disturbance at the inflow boundary; *b*, disturbance at the wall.

Therefore, it is of interest how our results from the direct Navier–Stokes simulations compare with theory and experiments and if they confirm any of the results of the various non-parallel theories. In this paper, results of the 4 calculation cases shown in figure 2 are discussed in detail. The horizontal bars in figure 2 indicate the four calculation cases. The beginning and end of the bars identify the actual location of the inflow and outflow boundary, respectively, of the integration domain used in the numerical simulation.

Thus, for example, case 1, with frequency parameter $F = 1.4 \times 10^{-4}$ should at first exhibit decay of the disturbances when proceeding in the downstream direction and then, inside the neutral loops in the region of instability, the disturbances should be amplified. Further downstream, after leaving the unstable region, disturbances should be damped again.

With increasing frequencies from case 1 to case 4 our numerical results should identify an increasing deviation from the stability behaviour of the standard parallel theory. For case 3 with $F = 2.6 \times 10^{-4}$ the flow should already be stable according to parallel theory. Case 4 with $F = 3.0 \times 10^{-4}$ is only unstable according to the non-parallel results by Saric & Nayfeh while it is stable according to Gaster, for both the first maximum of u' and the kinetic energy integral. Therefore, at this highest frequency, the biggest discrepancies should be expected between our Navier–Stokes results and parallel theory as well as the various non-parallel models.

To ensure that our results were of reliable accuracy and to allow a detailed quantitative comparison with results of the various theories, numerous test calculations with increased and decreased grid sizes $\Delta x, \Delta y$ were performed. In this way the effect of grid sizes on our results, in particular on amplitude distributions with respect to y and on growth rates, was investigated in detail (see Hoeptner 1981). Based on such investigations, grid sizes were selected for the calculations presented here that were small enough to ensure that the results are 'correct', in the sense that a further decrease of $\Delta x, \Delta y$ would only lead to insignificant changes in the numerical results.

The parameters used for the four calculation cases are summarized in table 1. For all four cases the reference Reynolds number was $Re = 10^5$, with, for example, $\bar{U}_\infty = 30$ m/s, $\bar{\nu} = 1.5 \times 10^{-5}$ m^2/s and $\bar{L} = 0.05$ m.

Typical results as they were obtained directly from our Navier–Stokes simulations for case 1 are shown in figures 3 and 4. There, the instantaneous disturbance quantities of u', v', and ω' are displayed in the entire (x, y) integration domain at a time instant after the disturbances have propagated through the entire integration domain and a time-periodic state is reached everywhere in the domain. Figure 3 shows the disturbance quantities u', v' in perspective representation with respect to

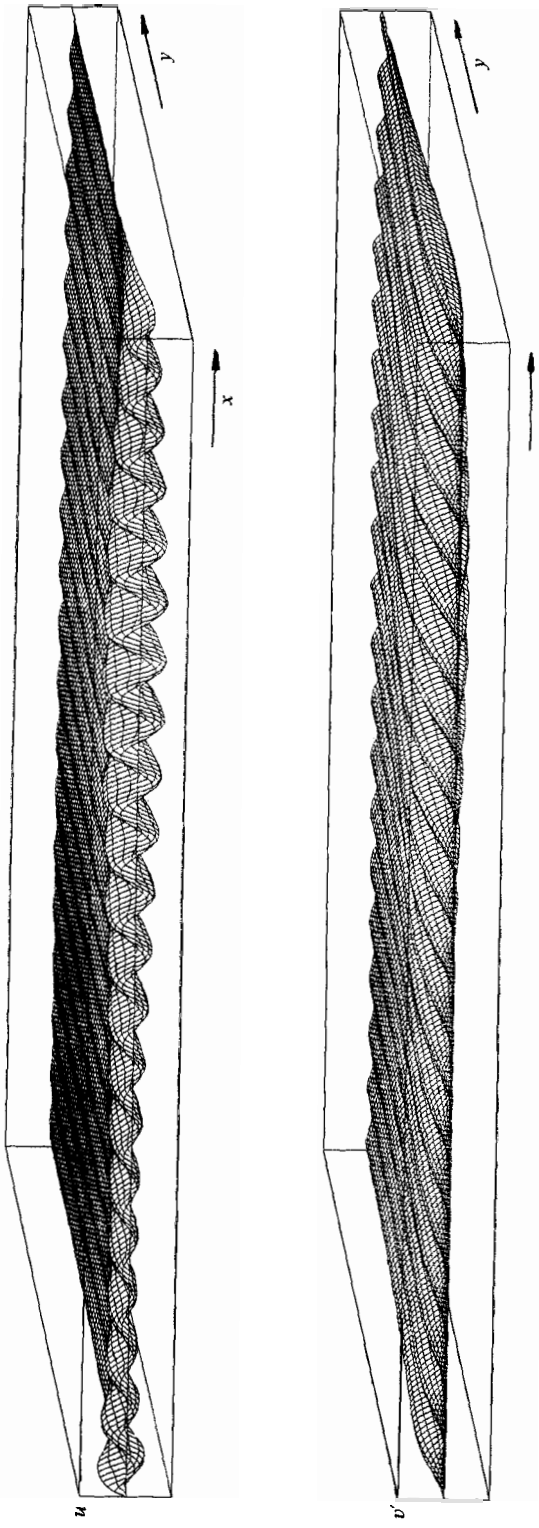

FIGURE 3. Instantaneous disturbance quantities u' and v' versus x and y (in perspective representation) for the entire integration domain after a time periodic state was reached (case 1).

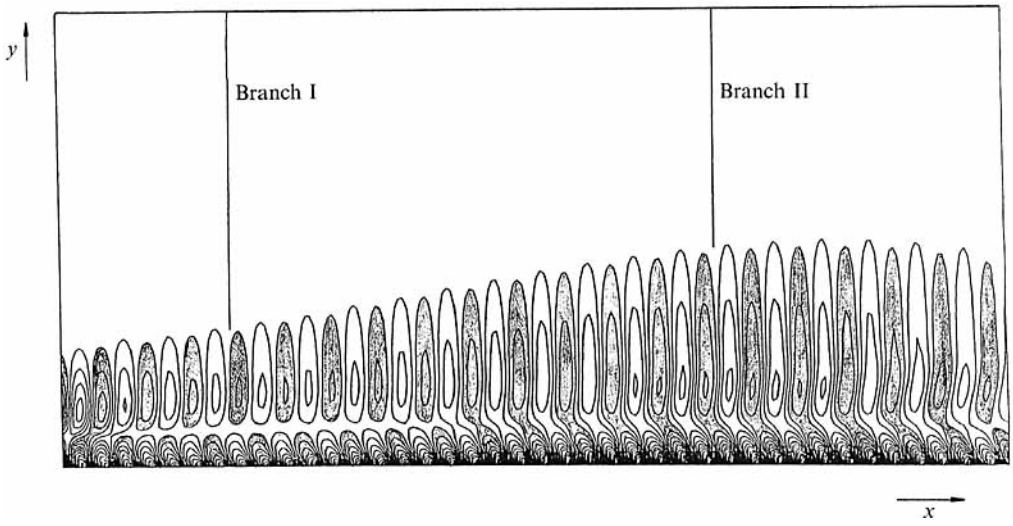

FIGURE 4. Isolines of disturbance vorticity ω' in the (x, y)-plane of the entire integration domain after the time periodic state was reached (case 1). Regions of negative ω' are shaded. Vertical bars indicate location of the neutral points of branch I and branch II, respectively, of the parallel linear theory.

x, y. In addition, in figure 4 the disturbance vorticity is presented in a contour plot of lines $\omega' =$ constant in the (x, y)-plane. These plots indicate already, at least in a qualitative manner, the stability behaviour for this case. Regions of stability (decay of the disturbances) and regions of instability (growth of the disturbances) can be clearly observed. For further analysis, the instantaneous data fields as displayed in figures 3 and 4 are processed to allow quantitative comparison with theoretical and experimental results.

For comparison with eigenfunctions of linear theory the data are Fourier analysed in time for every x and y location according to

$$u'(x, y, y) = u_0(x, y) + \sum_{i=1}^{K} (u_i(x, y) \cos(i\beta t + \Theta_{u_i})), \tag{3.1}$$

where $u_0(x, y)$ is the change of the mean flow.† Analogously this is done for v'. For the linear calculations considered here, only the first harmonic (or fundamental) is of interest, namely

$$u'(x, y, t) = u_1(x, y) \cos(\beta t + \Theta_{u_1}(x, y)). \tag{3.2}$$

Figure 5 shows the results of such a Fourier-analysis for case 1. The Fourier amplitudes are plotted with respect to x, y in perspective representation as in figure 3. From the amplitude distributions for all x-stations, such as shown in figure 5, growth curves for any quantity can be determined. From the growth curves amplification rates can be extracted for comparison with both parallel and non-parallel theories and experimental measurements.

3.1. *Amplitude distributions*

Amplitude distributions (Fourier amplitudes versus distance from the wall) of the disturbance velocity components u' and v' for the calculation case 1 and 4 are plotted in figures 6 and 7. These amplitude distributions can be directly compared with the

† u_0 is the deviation of the time-averaged Navier–Stokes solution and the solution of the steady Navier–Stokes equations. Thus this deviation is due to nonlinear interactions. For the present calculations u_0 is therefore very small and can be neglected.

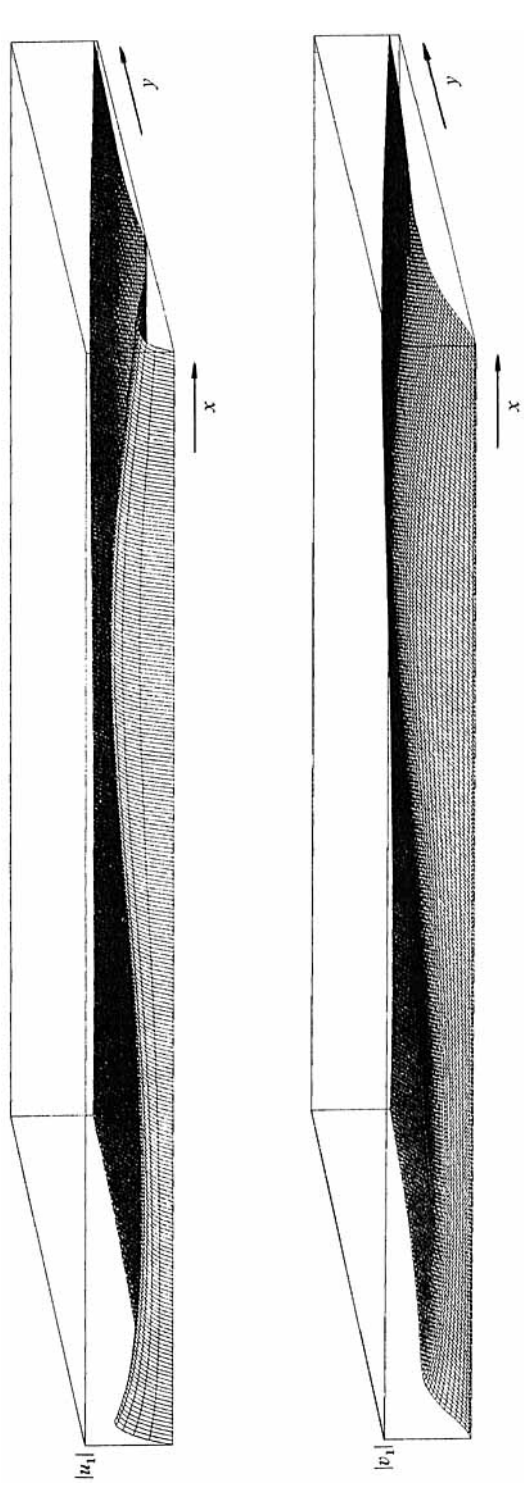

FIGURE 5. Fundamental Fourier amplitude of the u'- and v'-disturbances versus x and y (in perspective representation) for the entire integration domain (case 1).

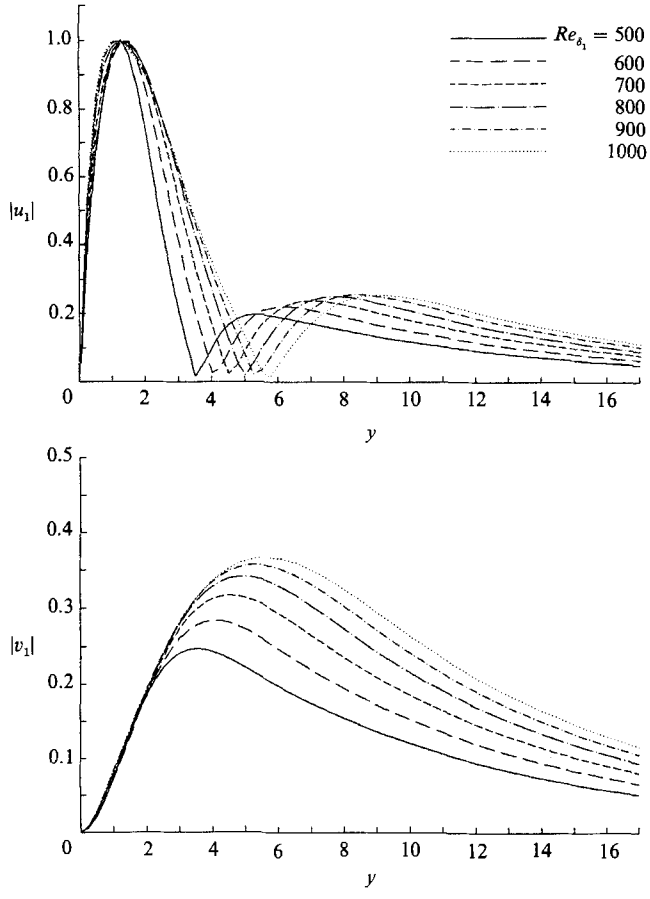

FIGURE 6. Fourier amplitudes (normalized by the maximum of u') versus y of the u'- and v'-disturbances for various downstream locations Re_{δ_1} (case 1, $F = 1.4 \times 10^{-4}$).

eigenfunctions obtained from linear stability theory. In figure 6 the amplitudes are plotted versus y and in figure 7 versus a normalized coordinate $y^* = y/\delta_1$ (δ_1 is the local displacement thickness). The amplitudes are normalized such that the first maxima of u' are equal to 1. Thus, with normalization factor $k = 1/u'_{\max_1}$ the actual amplitudes are related to the normalized ones shown in figures 6 and 7 such that $u' = u'_{\text{norm}}/k$ and $v' = v'_{\text{norm}}\,(Re)^{\frac{1}{2}}/k$ where the subscript 'norm' denotes the normalized quantities. From figures 6 and 7 one can observe that with changing Re_{δ_1} (that is, for different downstream locations) not only the locations of the maxima and of the zero values are shifted but, in addition and in spite of the normalization, the amplitude values can vary considerably at other y locations. This is particularly true for the v' distributions. It is also obvious from these figures that the variation of the normalized amplitude distributions is significantly different for the two representations, depending on whether they are plotted with respect to y or y^*.

From these observations it is already clear that amplification rates would be strongly dependent on the criteria used. For example, from figure 6 one would obtain disturbance growth in x over a wide range of y for both u' and v'. Although based on the inner maximum of u' the flow would be judged to be neutrally stable, the growth rates would be very strong beyond the corresponding maxima. This is also true for v' in figure 6. In contrast, in figure 7 this behaviour is significantly

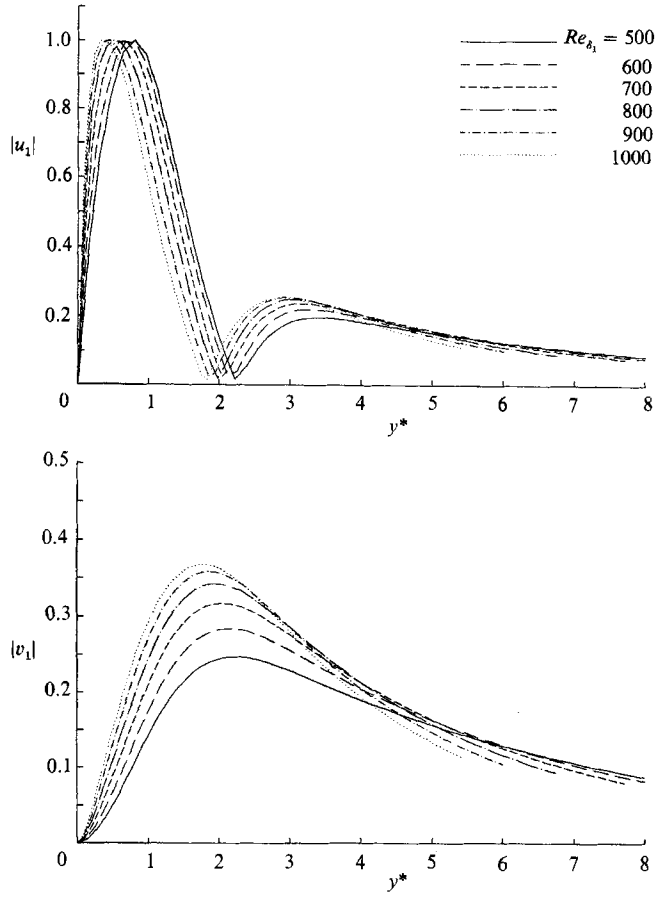

FIGURE 7. Fourier amplitudes (normalized by the maximum of u') versus y^* ($y^* = y/\delta_1$) of the u'- and v'-disturbances for various downstream locations Re_{δ_1} (case 1, $F = 1.4 \times 10^{-4}$).

different. Based on the u' distributions, for wide ranges of y, the amplitudes decrease when passing downstream at constant y^* (for example beyond the first maxima and below the zero locations) and therefore the flow could be termed stable, if only the behaviour at these y^* locations were to be considered. However, at other y^* locations this behaviour is opposite with the disturbances growing in the downstream direction. A similar behaviour can be observed for the v' component in figure 7. The corresponding plots for the other calculation cases, which are not shown here, exhibit a similar qualitative behaviour to that observed in figures 6 and 7.

How do the amplitude distributions of the Navier–Stokes solution compare with linear stability theory? In figure 8 the amplitudes of our Navier–Stokes calculations for case 1 are plotted together with the eigenfunctions obtained from (parallel) linear stability theory calculations (Kümmerer 1973; these linear stability results are practically identical to those of Jordinson 1970). For plotting the amplitudes in figure 8 the same normalization is used as before so that the inner maxima of u' are equal to 1. The good agreement between the Navier–Stokes solution and linear stability theory results is indeed remarkable. Comparison for the other cases is omitted here, owing to lack of space; however, the agreement is in all cases of the same quality as for case 1. This good agreement supports the assumption made in

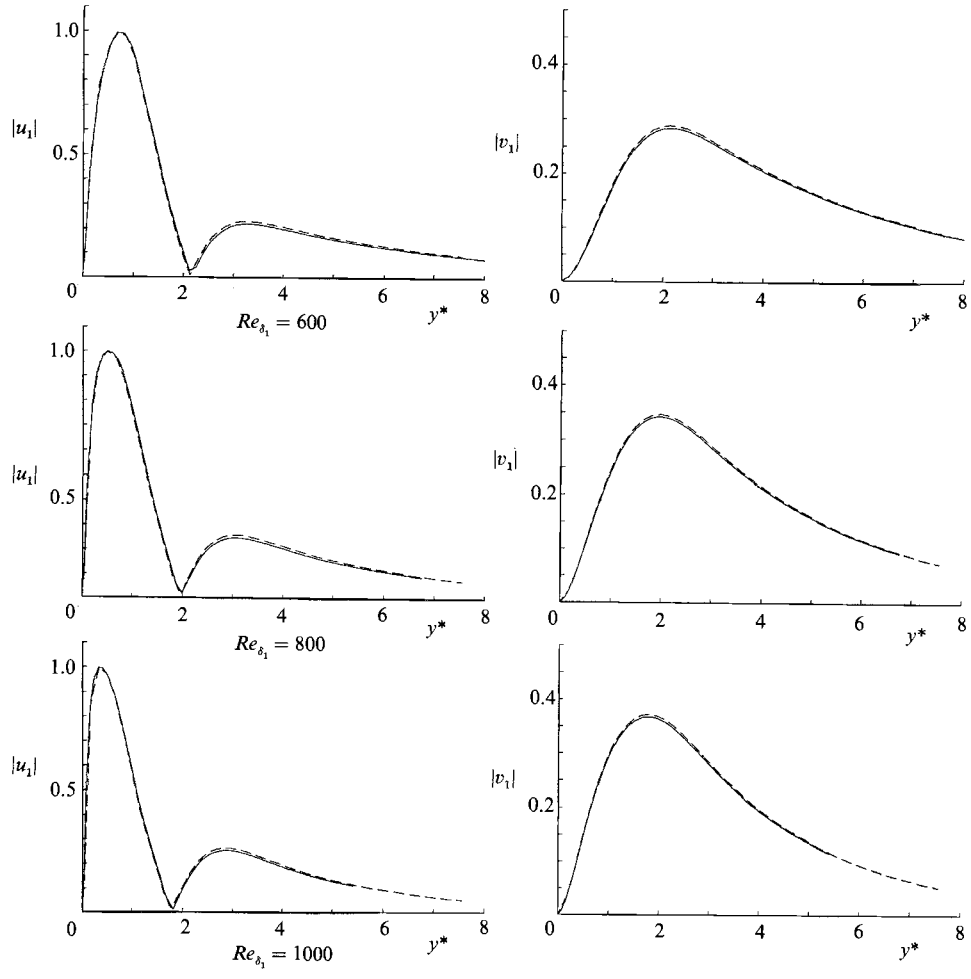

FIGURE 8. Comparison of the amplitude distributions (normalized by the maximum of u') for u' and v' of the Navier–Stokes calculations (——) with those of the parallel linear stability theory (– – –) for various Re_{δ_1} (case 1, $F = 1.4 \times 10^{-4}$).

non-parallel theory that the non-parallel effects on the eigenfunctions are negligible (of order $Re^{-\frac{1}{2}}$).

Bridges & Morris presented non-parallel corrections of the eigenfunctions of the linear stability theory (their figure 5). In figure 9 the real and imaginary parts of the amplitudes from the Navier–Stokes solution and eigenfunctions of the linear stability theory are compared. The deviations between the Navier–Stokes solution and the linear stability theory are of similar magnitude as in Bridges & Morris. However, for the imaginary part of the eigenfunction, the correction as suggested by the Navier–Stokes solution is in the opposite direction to that of Bridges & Morris.

3.2. *Spatial-disturbance amplification*

The results presented in figures 6 and 7 suggested already that the magnitude of the spatial growth of the disturbances was strongly dependent on the specified y or y^* location or on which variable would be considered. For other criteria, such as local kinetic energy e, kinetic energy integral E etc. the behaviour would again be different altogether.

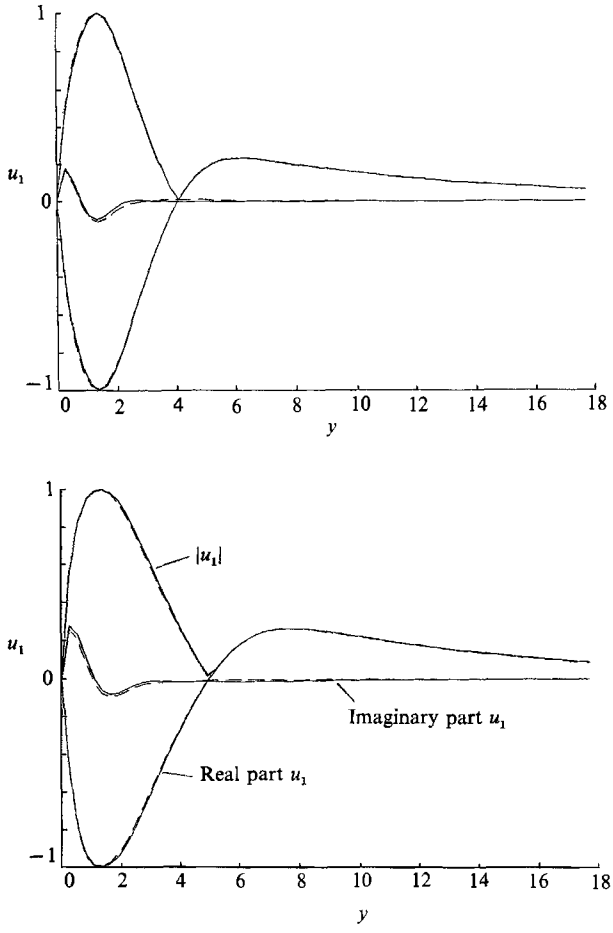

FIGURE 9. Comparison of real and imaginary parts of the amplitude distribution as well as the total amplitude distribution (normalized by the maximum of u') of the Navier–Stokes calculation (——) with the parallel linear stability theory (– – – –) for $Re_{\delta_1} = 600$ and $Re_{\delta_1} = 800$ (case 1, $F = 1.4 \times 10^{-4}$).

To shed light on how different criteria affect the spatial-amplitude behaviour, results based on our Navier–Stokes calculations will be presented and discussed here. The effects of the following criteria were investigated:

(*a*) $u_{\max_1}$: inner (first) maximum of the u' amplitude distribution;
(*b*) $u_{\max_2}$: outer (second) maximum of the u' amplitude distribution;
(*c*) $v_{\max}$: maximum of the v' amplitude distribution;
(*d*) $\omega_{\max_1}$: wall (first) maximum of the ω' amplitude distribution;
(*e*) $\omega_{\max_2}$: outer (second) maximum of the ω' amplitude distribution;
(*f*) $\int_0^\infty |\omega'| \, dy$: time-averaged absolute value of ω' integrated over the entire boundary layer;
(*g*) $\int_0^\infty \overline{u}'^2 \, dy$: contribution of the u'-component to the kinetic-energy integral;
(*h*) $\int_0^\infty \overline{v}'^2 \, dy$: contribution of the v'-component to the kinetic-energy integral;
(*i*) $\int_0^\infty (\overline{u}'^2 + \overline{v}'^2) \, dy$: kinetic energy integral;
(*j*) following lines y = constant;

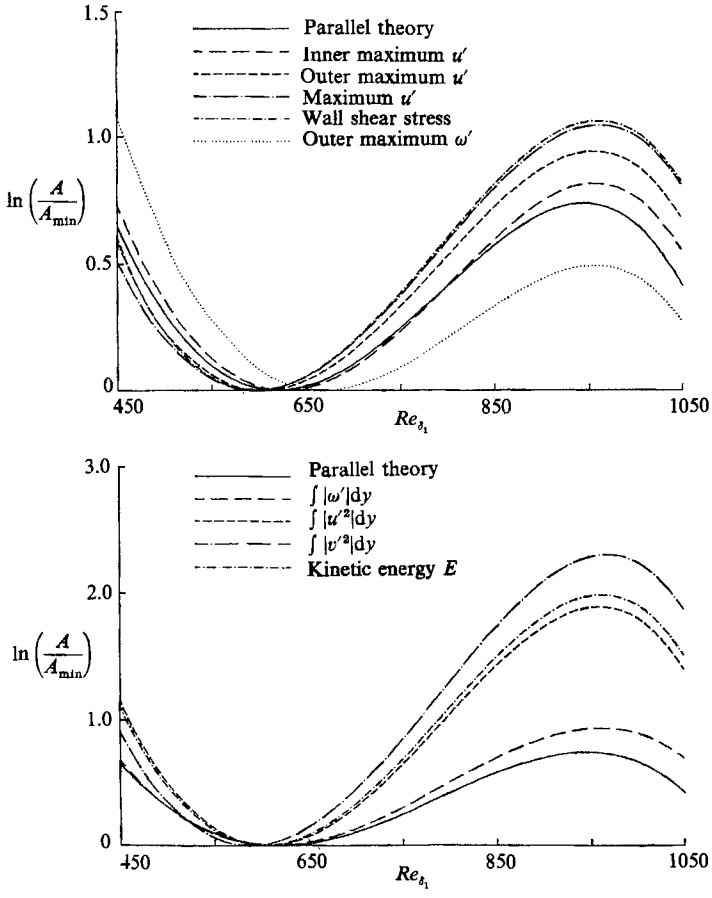

FIGURE 10. Normalized amplification curves of the Navier–Stokes calculation (case 1, $F = 1.4 \times 10^{-4}$) for various criteria in comparison with the parallel linear stability theory.

(*k*) following lines η = constant ($\eta = y/(2x)^{\frac{1}{2}}$, boundary-layer coordinate, $\eta = 1.21677y^*$).

The maxima of the amplitude distributions required for some of the criteria above were determined from the discrete amplitude functions by use of spline interpolations. For the evaluation of the integrals from 0 to ∞ for items (*g*), (*h*) and (*i*) the condition for exponential decay (equation (2.16)) was employed to continue the integration outside the Navier–Stokes integration domain.

Amplification curves for $\ln(A/A_{\min})$ versus Re_{δ_1} for various stability criteria are plotted in figure 10. The amplitudes are normalized by their respective minimum values so that the normalized curves have relative minima for 1. For comparison, the amplification curve of parallel linear theory is also shown in figure 10. This curve is obtained by integrating in the x-direction considering that α_i (dimensionless with the displacement thickness δ_1) is a function of x (from linear theory) using the relationship

$$\ln\frac{A}{A_0} = -\int_{x_0}^{x} \frac{\alpha_i(x)}{\delta_1(x)}\,\mathrm{d}x. \tag{3.3}$$

It can be observed that for all criteria, except for the second maximum for ω', growth rates are higher than those of linear theory. The very strong effect of the various criteria on the final amplitudes attained at branch II is indeed remarkable.

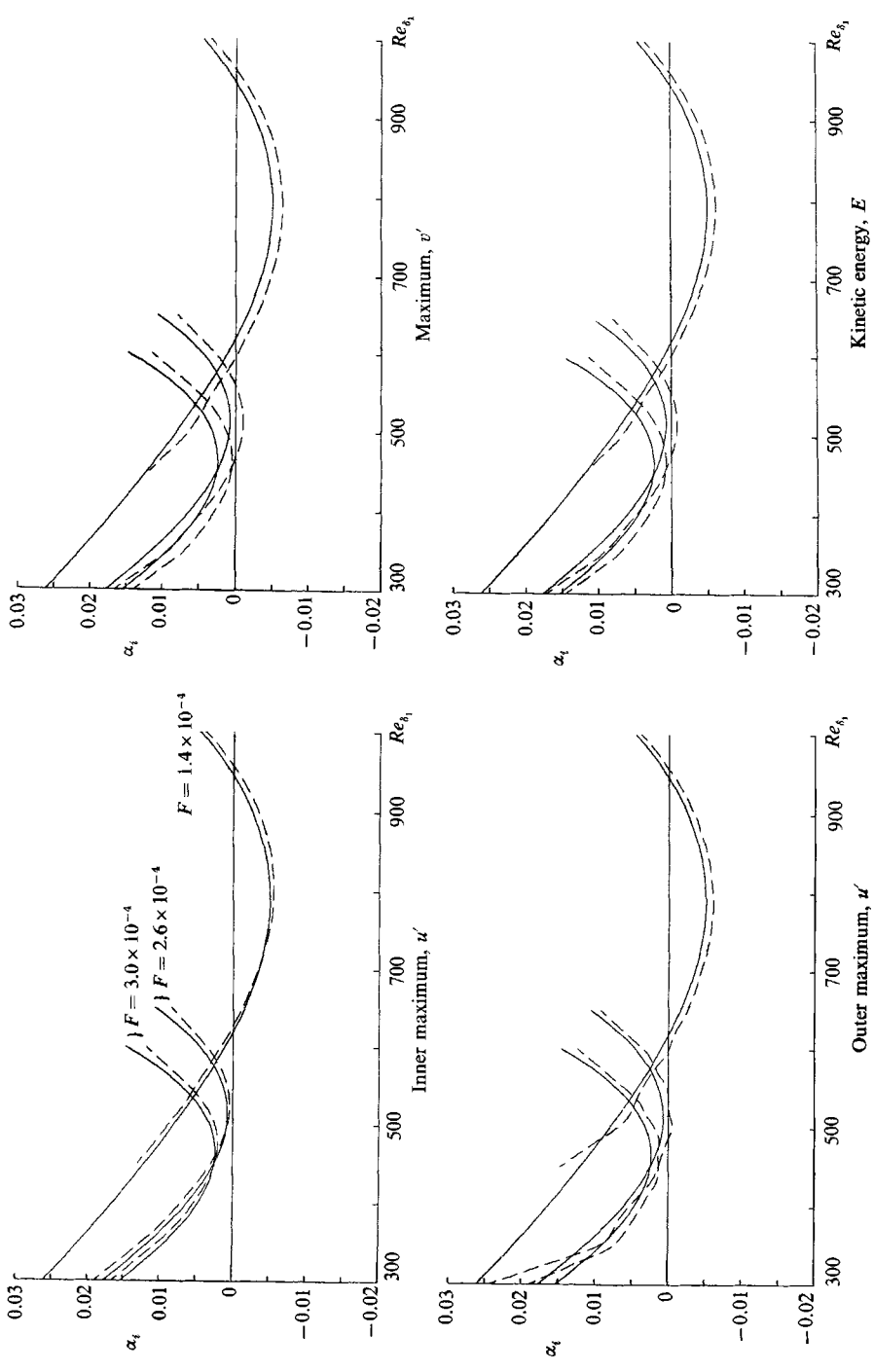

FIGURE 11. Growth rates α_i obtained from the Navier–Stokes calculations for various criteria for $F = 1.4 \times 10^{-4}$, $F = 2.6 \times 10^{-4}$ and $F = 3.0 \times 10^{-4}$ (——) (cases 1, 3 and 4). Comparison with growth rates α_i of parallel linear stability theory (——).

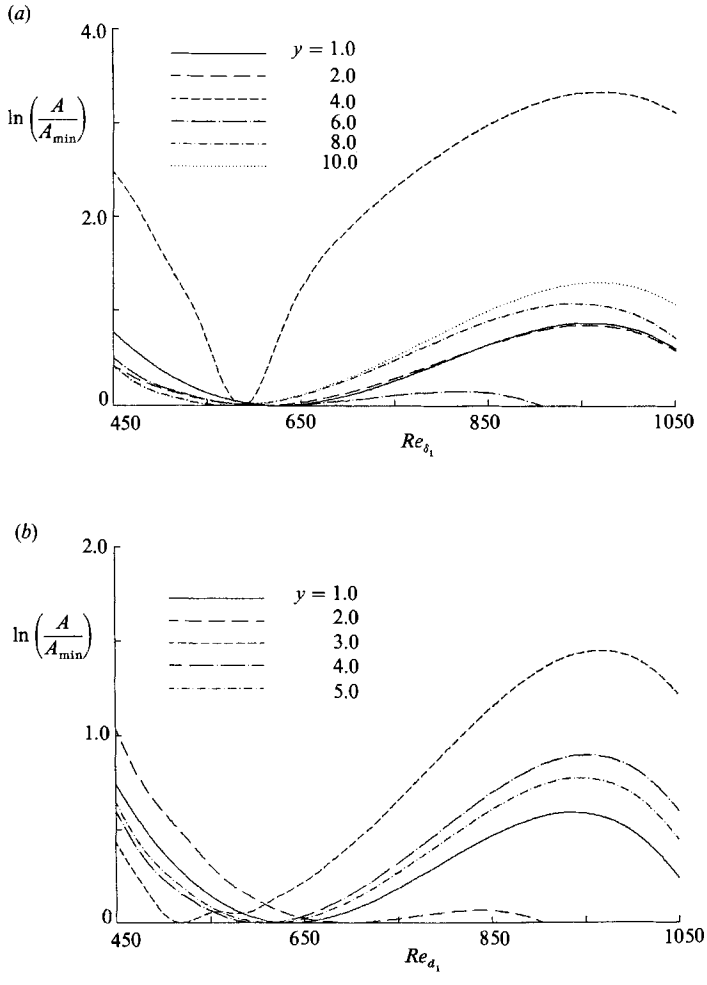

FIGURE 12. Normalized amplification curves of the Navier–Stokes calculation (case 1, $F = 1.4 \times 10^{-4}$) for following the u'-disturbance in the downstream direction at (*a*) constant y or (*b*) at constant η.

From amplification curves such as shown in figure 10 the neutral points of our Navier–Stokes calculations can be determined by identifying the maxima and minima. Also the growth rates α_i of the Navier–Stokes solution are determined from such amplification curves using the formula

$$\alpha_i = -\frac{\mathrm{d}(\ln(A/A_0)}{\mathrm{d}x}\delta_1(x). \tag{3.4}$$

To allow a meaningful comparison, growth rates α_i which are determined from growth curves based on criteria with quadratic terms, such as $\int_0^\infty \overline{u'^2}\,\mathrm{d}y$, are multiplied by a factor $\frac{1}{2}$.

A quantitative comparison of the growth rates obtained from amplification curves such as shown in figure 10 is given in figure 11. To determine the growth rates, equation (3.4) was employed where the differentiation is carried out numerically using a least-square fit method with piecewise fitted polynomials of second order.

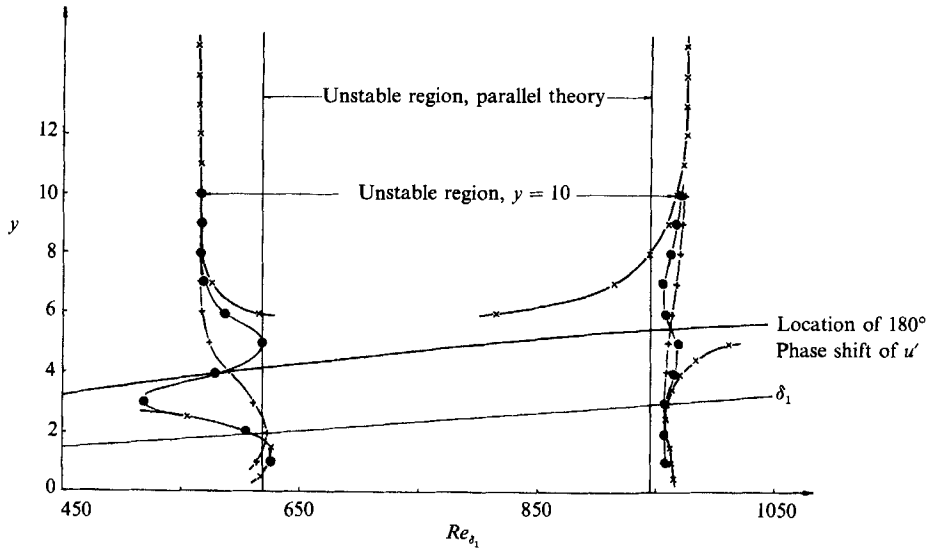

FIGURE 13. Locations of the neutral points in the (y, Re_{δ_1})-plane when following the disturbance at constant y (case 1, $F = 1.4 \times 10^{-4}$); $\times$, u'-disturbance; $+$, v'-disturbance; ●, local kinetic energy.

Results are shown for cases 1, 3 and 4. The growth rates α_i are plotted versus Re_{δ_1} for different criteria, and are compared with the α_i of parallel linear stability theory. The curves obtained from the Navier–Stokes solution for the second maximum of u' are somewhat wavy. This is due to the numerical differentiation. The u'-values for the second maximum are already very small, in particular for cases 3 and 4 with no amplification, so that numerical round-off errors start to play a role.

From figure 11 one can observe that for all criteria shown, except for the first maximum of u', the α_i-values of our Navier–Stokes solution are consistently smaller than those of the parallel theory, thus resulting in a larger disturbance amplification in the Navier–Stokes solution than in the parallel linear stability theory. For the first maximum of u' the α_i-values of the Navier–Stokes solution are at first slightly larger, and further downstream smaller, than the α_i of the parallel linear theory. The deviations of the non-parallel results from the linear stability results show for all criteria qualitative similarity that is independent of the disturbance frequency.

In experimental investigations the stability criteria are often based on the amplitude behaviour along lines of constant physical distance from the wall (y = constant) or along lines of constant η. In figure 12 typical amplification curves for u' are shown, based on constant y and constant η, respectively (normalized with their respective minimum values). It is obvious that drastically different results are obtained depending on whether the curves are versus η or y and depending on which values are used for y or η. In particular, the neutral points are also shifted considerably depending on the chosen y or η position. This effect is summarized in figures 13 and 14 where, for case 1, the locations of the neutral points are plotted for the two situations of following the disturbance at either y = constant or η = constant. In these figures the neutral positions are shown for the u'-disturbance, the v'-disturbance and for the local kinetic energy of the disturbance $e = \overline{u'^2} + \overline{v'^2}$. For comparison, the neutral locations ($\alpha_i = 0$) of the linear stability theory are also shown. It is now obvious that the upstream and/or downstream shift of the neutral points, with different constant y or η, is considerable. Especially for the u'-

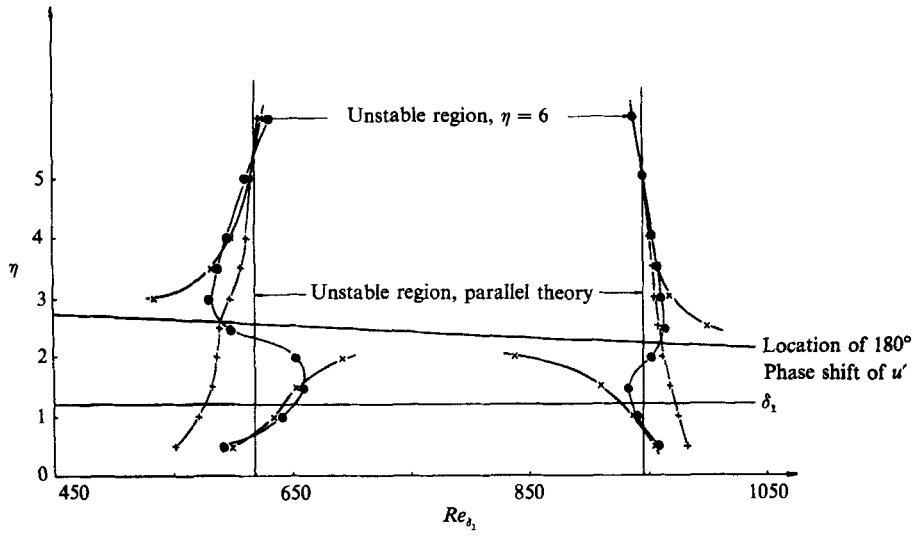

FIGURE 14. Locations of the neutral points in the (η, Re_{δ_1})-plane when following the disturbance at constant η (case 1, $F = 1.4 \times 10^{-4}$); ×, u'-disturbance; +, v'-disturbance; ●, local kinetic energy.

disturbance an ambiguous behaviour exists as the y or η location of the 180° phase shift (of the u' eigenfunction) is approached. In figure 13 for y = constant, approaching the 180° phase-shift location from the wall, the unstable region increases more and more. Approaching the 180° phase-shift location from the edge of the boundary layer the unstable region appears to shrink towards zero. For the representation with following on lines η = constant in figure 14 this behaviour is exactly opposite.

From this it is obvious that, if the stability behaviour is to be judged by following the u'-disturbance in the downstream direction at constant y or constant η, it is essential to stay away from the 180° phase-shift location. For the local kinetic energy, as also shown in figures 13 and 14, the variation of the location of the neutral points is still considerable, yet the ambiguity close to the 180° phase-shift point is no longer present. From figure 13, one can also observe that the non-parallel effects on the location of the neutral points when following on lines y = constant are strongest within approximately four displacement thicknesses and are practically negligible further away from the wall.

3.3. *Comparison with non-parallel theories and experiments*

While the question is still unresolved as to what criterion should best be used for defining stability it is of the utmost importance, however, that for comparison among various theories and in particular for comparison of theory and experiment, identical criteria are used.

As discussed previously, taking the effect of the non-parallel base flow into consideration, as in the various non-parallel theories, results in growth rates which are strongly dependent on the underlying criteria. This effect is mainly due to the fact that the eigenfunctions change with the x-location and to a lesser degree due to a possible change of the eigenvalue α_i itself. A comparison of the growth rates versus x of our Navier–Stokes results with results of the non-parallel theory by Gaster are shown in figure 15. Results are shown for three criteria, namely for the

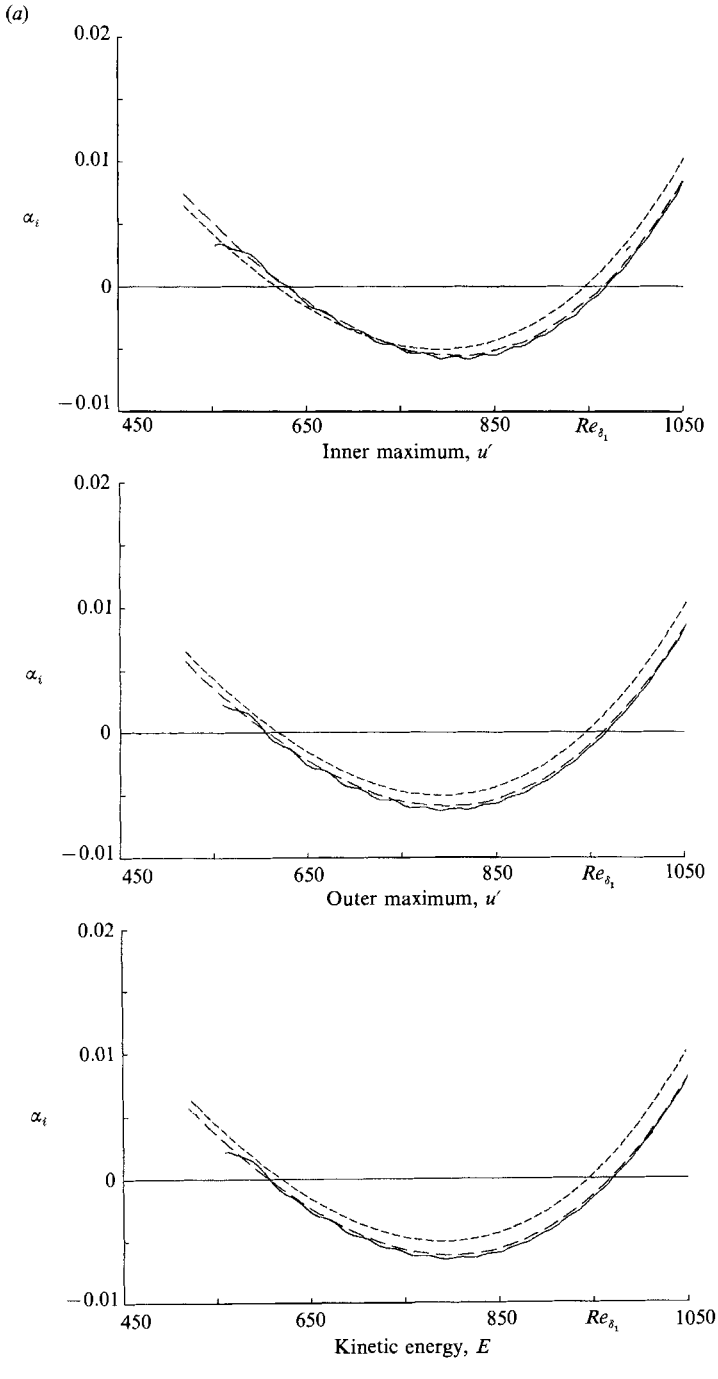

FIGURE 15(a). For caption see facing page.

inner maximum of u', for the outer maximum of u' and the kinetic energy $E = \int_0^\infty (\bar{u}'^2 + \bar{v}'^2)\,dy$, and for two different frequencies $F = 1.4 \times 10^{-4}$ and $F = 3.0 \times 10^{-4}$ (cases 1 and 4; disturbance generation is by blowing and suction, see §2.2). For reference, the curves from standard parallel (spatial) theory are shown

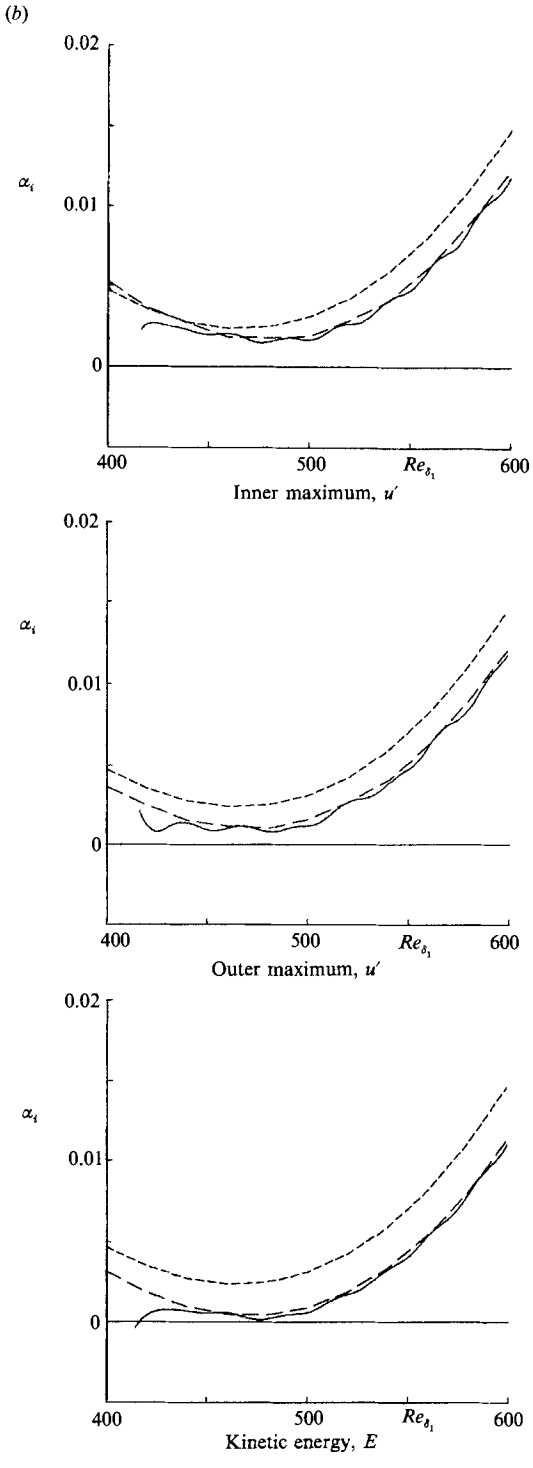

FIGURE 15. Comparison of growth rates α_i of the Navier–Stokes solution (——) with the parallel linear stability theory and the non-parallel theory by Gaster (1974) for various criteria. (*a*) Case 1, $F = 1.4 \times 10^{-4}$; (*b*) case 4, $F = 3.0 \times 10^{-4}$.

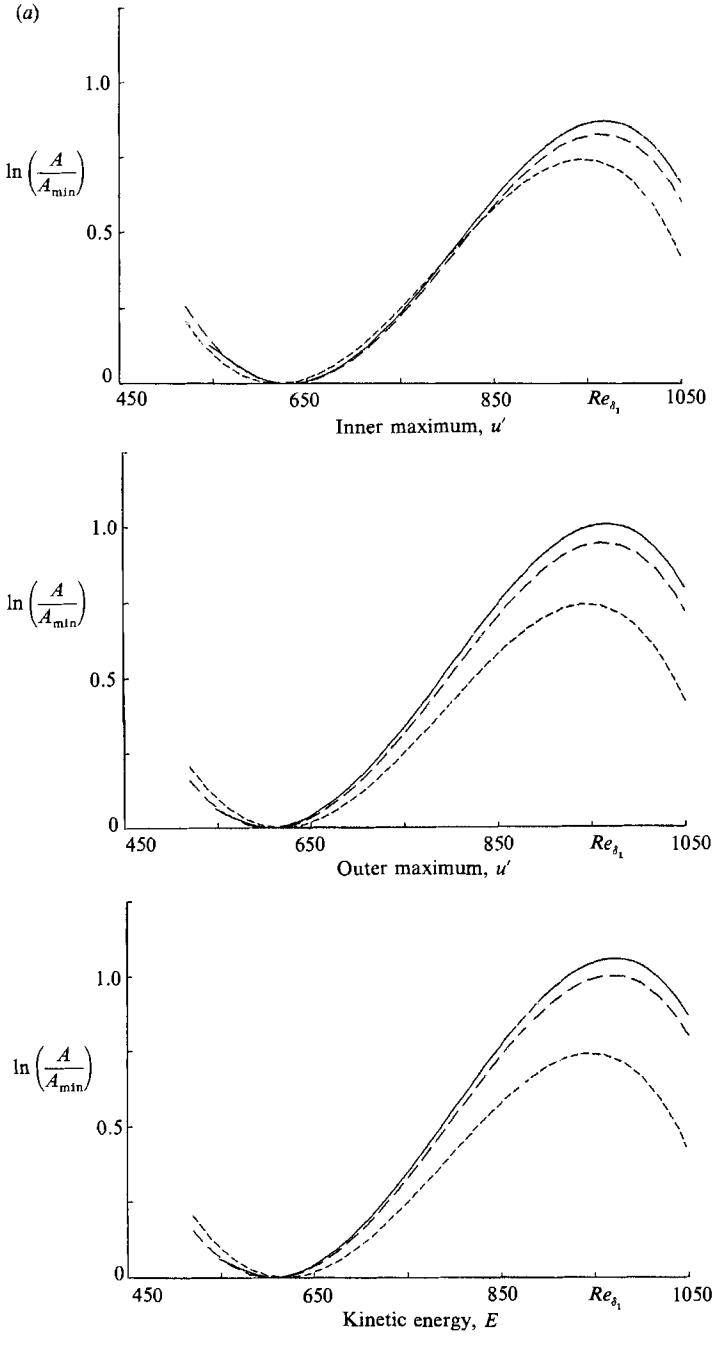

FIGURE 16(a). For caption see facing page.

also. It is obvious that for all cases and for all criteria, comparison between the Navier–Stokes solution and the non-parallel theory by Gaster is remarkable. For all other calculation cases not shown here agreement with the theory by Gaster is as for case 1 and 4. Almost immediately downstream of the disturbance generation the curves practically coincide (the local solution close to the disturbance generation is

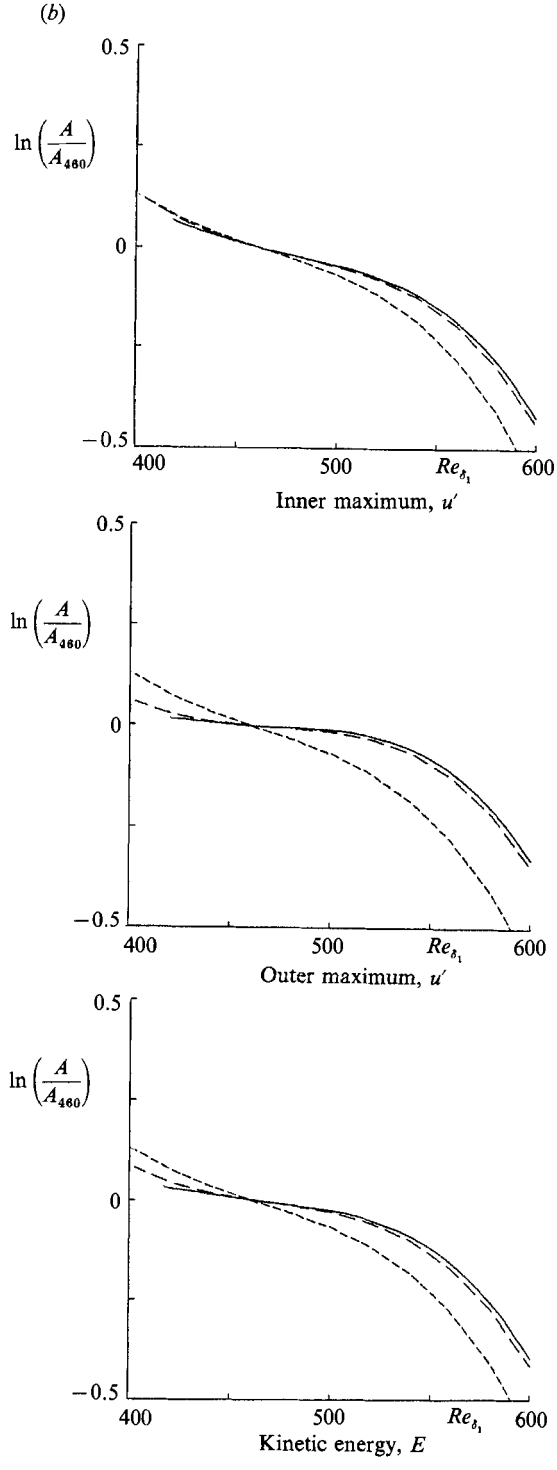

FIGURE 16. Comparison of amplification curves of the Navier–Stokes solution (——) with the parallel linear stability theory (----) and the non-parallel theory by Gaster (1974) (– – –) for various criteria (disturbances generated by localized blowing and suction). (*a*) case 1, $F = 1.4 \times 10^{-4}$, normalized by the minimum amplitude; (*b*) case 4, $F = 3.0 \times 10^{-4}$, normalized at $Re_{\delta_1} = 460$.

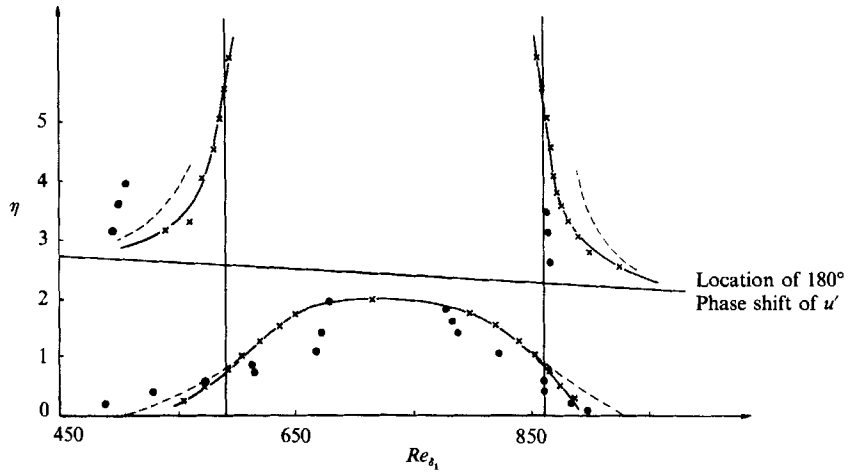

FIGURE 17. Location of the neutral points in the (η, Re_{δ_1})-plane when following the disturbances at constant η. Comparison of the Navier–Stokes solution (case 2, $F = 1.56 \times 10^{-4}$) (×) with experimental measurements by Kachanov *et al.* (1979) (●) and the non-parallel theory by Saric & Nayfeh (1975) (----).

not shown). The slight wavyness is due to the numerical differentiation which is required to determine the growth rates from the amplification curves using equation (3.4). In contrast to the growth rate curves shown previously in figure 11, here no smoothing is employed. Rather, the data are calculated directly in order to allow an unbiased comparison. The amplification curves of the Navier–Stokes solution versus Re_{δ_1} from which the growth rates are determined are shown in figure 16. For comparison, amplification curves obtained from the non-parallel theory by Gaster and from linear stability theory are shown also. As before, the agreement between the Navier–Stokes solution and the non-parallel theory by Gaster is very good, while the deviation from the parallel theory appears quite significant.

Kachanov *et al.* (1979) experimentally investigated the non-parallel effects. The location of the neutral points for $F = 1.56 \times 10^{-4}$ obtained from these experiments by following the development of the u'-disturbances at constant η are plotted in figure 17 in the (η, Re_{δ_1})-plane as in figure 14 for case 1. For comparison, the neutral locations as obtained from our Navier–Stokes calculation for case 2 are shown together with the results of the non-parallel theory by Saric & Nayfeh (1977). The locations of the phase reversal for u' as determined from the experiments and the Navier–Stokes calculations are plotted also. Below the 180° phase-shift location the agreement between the Navier–Stokes results and experiments, as well as with the non-parallel results by Saric & Nayfeh, is quite reasonable when considering the difficulties in accurately determining the neutral location from experimental measurements. However, close to the wall the theory by Saric & Nayfeh consistently predicts lower-Reynolds-number neutral locations (for branch I) and higher-Reynolds-number neutral locations (for branch II) than our Navier–Stokes results. Above the 180° phase-shift location, agreement between Navier–Stokes, non-parallel theory, and measurement is much less satisfactory. The non-parallel results by Saric & Nayfeh predict neutral locations at higher Reynolds numbers than the experiments for both branch I and branch II. Our Navier–Stokes calculations yield neutral locations that are at higher Reynolds numbers for branch I and at lower Reynolds numbers for branch II than those obtained from the non-parallel theory by Saric &

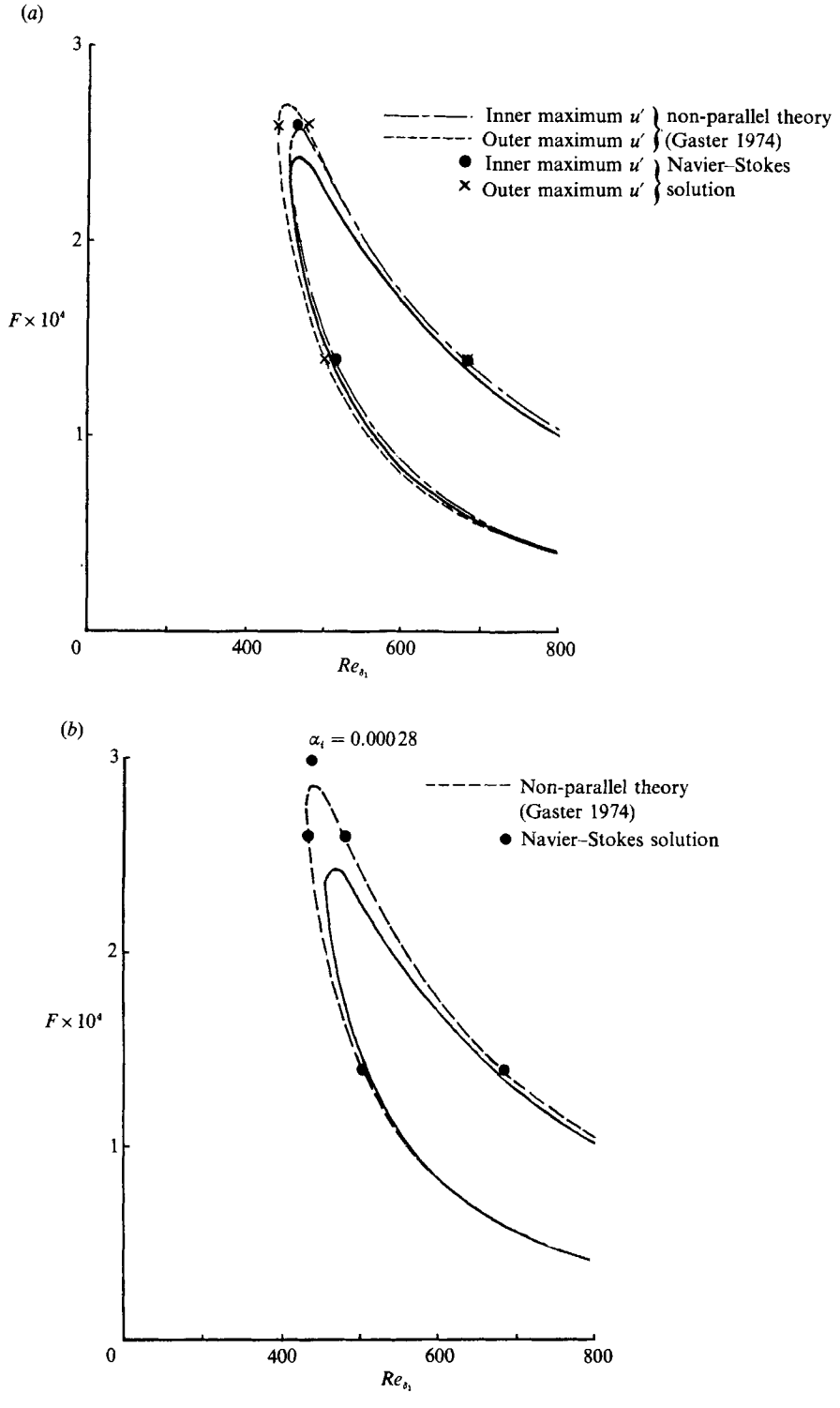

FIGURE 18(*a*, *b*). For caption see facing page.

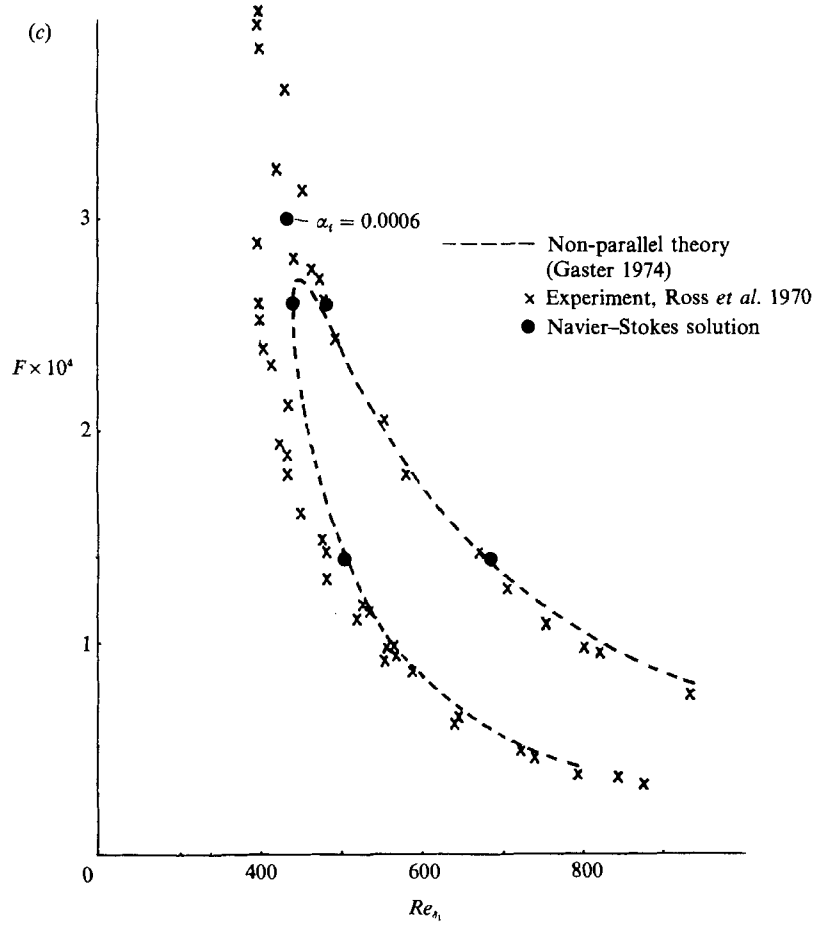

FIGURE 18. Neutral locations obtained from the Navier–Stokes calculations for cases 1, 3 and 4 together with the neutral curves of the parallel linear stability theory (——) and of the non-parallel theory by Gaster (1974) for various criteria: (*a*) inner and outer maximum of u', (*b*) kinetic energy integral E, (*c*) u' at $y/\delta = 0.15$, comparison with experiment of Ross *et al.* (1970). *Note*: in the figure caption for the inner and outer maximum of u' in Gaster's (1974) paper the notations should be interchanged (Gaster, private communication.)

Nayfeh. Thus, for this criterion (η = constant), the unstable region obtained from our Navier–Stokes-calculations would always be somewhat smaller than that of the non-parallel theory by Saric & Nayfeh.

In figures 18 and 19 neutral points obtained from the Navier–Stokes calculations are shown together with the neutral curves for various non-parallel theories. For comparison, the neutral curve of the standard parallel theory is given also. Figure 18(*a*) shows the neutral curves obtained by Gaster for the inner and outer maximum of the u'-disturbances. For the neutral points based on the kinetic energy E, as obtained from the Navier–Stokes solution, agreement with the neutral points by Gaster is equally good (figure 18*b*). Here, case 4 of our calculation just barely yields a neutral location.

How do our neutral points compare with those obtained experimentally ? In figure 18(*c*) the neutral points of the Navier–Stokes calculation using the same criteria as for the experimental points, namely $y/\delta = 0.15$, are compared with those of Ross

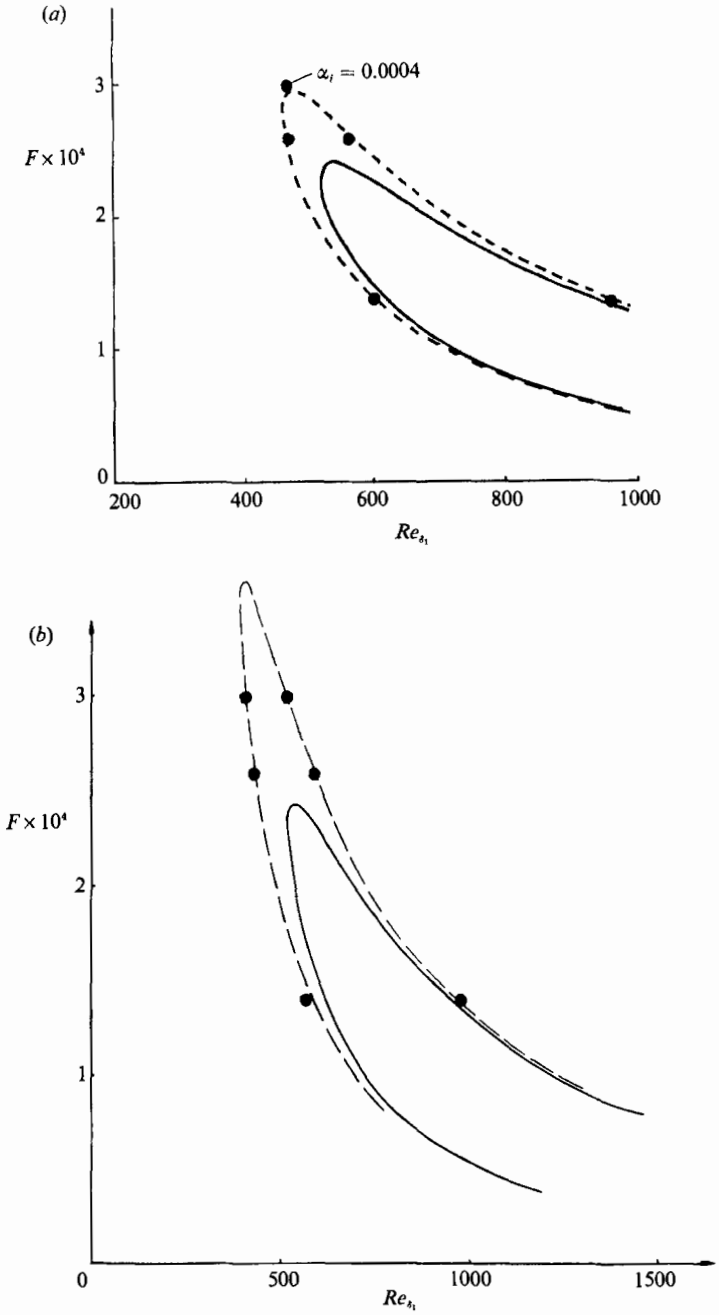

FIGURE 19. Examples of fortuitous agreement between the neutral points obtained from simulations for one flow quantity and theoretical predictions based on another. Neutral locations obtained from the Navier–Stokes calculations for the cases 1, 3 and 4 (●) together with the neutral curves of the parallel linear stability theory (——) and of the non-parallel theories: (*a*) ---, Bridges & Morris (1987), criterion: maximum of v'; (*b*) ——, Saric & Nayfeh (1975), criterion: inner maximum of u', compared with Navier–Stokes solution, criterion: u' at $y = 10$.

et al. and the corresponding neutral curve by Gaster. It is obvious that the neutral points obtained from the Navier–Stokes calculation still differ significantly from the experimental neutral location. On the other hand the Navier–Stokes neutral points almost coincide with the neutral curve by Gaster.

In their paper, Bridges & Morris (1987) displayed a neutral curve based on the concept that there exists a unique definition of the non-parallel effects on the wavenumber that is independent of the effects of streamwise variation of the wavenumber. Coincidentally, this is the same total result as would be obtained if the maximum of the v'-fluctuation were considered. Therefore neutral points obtained from our Navier–Stokes calculations for the maximum v' should be directly comparable with the neutral locations as obtained from this theory. In figure 19(*a*) the neutral curve of Bridges & Morris is shown together with the neutral location obtained from calculations 1, 3 and 4. The neutral points of our Navier–Stokes solution based on the same criteria practically coincide with the neutral points obtained from the non-parallel analysis. Finally in figure 19(*b*) the neutral loop obtained by Saric & Nayfeh is reproduced. It yields an unstable region that is larger than any of the neutral loops shown so far. In their first paper Saric & Nayfeh (1975) did not define the underlying criterion. In the later paper (Saric & Nayfeh 1977) they argued that their neutral curve would be for the inner maximum of u'. The neutral points for the inner maximum of u', as displayed in figure 18(*a*), deviate considerably from these results. Therefore we searched for another criterion that could possibly yield an unstable region as large as the one given by Saric & Nayfeh. As is obvious from figure 13, using u', v' or the local kinetic energy far away from the wall (at least $5\delta_1$) and following the disturbances downstream at constant y, yields a larger unstable region than using, for example, the inner maximum of u' as a criterion. These neutral points are also displayed in figure 19(*b*) and, as can be observed, almost coincide with the neutral points of Saric & Nayfeh. However, to make it clear, this agreement is indeed fortuitous, because the theoretical neutral curve was obtained for the inner maximum of u' as the underlying criterion.

In summary, our Navier–Stokes calculations confirm that the discrepancy between the experimental neutral locations and the parallel linear-stability theory cannot be explained by non-parallel effects. Therefore, other effects must be responsible such as, for example, (*a*) a very small adverse pressure gradient, (*b*) the disturbance source (vibrating ribbon) too close to the neutral location and (*c*) nonlinear effects. With regard to (*a*) it is well known that adverse pressure gradients are strongly destabilizing and that only small pressure gradients would be required to enlarge the unstable region such as defined by the experimental measurements by Ross *et al.* In experiments it is very difficult to accurately maintain a uniform pressure gradient. Possible reasons for (*b*) and (*c*) are the facts that the growth rates for the higher frequencies (where the deviations between theory and experiments are most significant) are getting very small. In order to obtain reliable signal responses that are not totally obscured by the background turbulence, the experimenter has two choices: either he can (virtually) move the disturbance source closer to the branch I location (so as to minimize disturbance decay in the stable region) or he can increase the disturbance amplitude. Therefore, the neutral location would be affected if the disturbance source is too close to the branch I location. If input amplitudes are too big, nonlinear effects, both two- and three-dimensional, may play a role and thus influence the neutral location. However, our nonlinear Navier–Stokes calculations (Konzelmann 1983) using larger amplitude two-dimensional disturbances have shown, that two-dimensional nonlinear effects have a minimal influence on the

neutral locations, especially for branch I, when disturbance amplitudes u'/U_∞ are smaller than 2%. Therefore, it is unlikely that the discrepancy between experiments and theory can be explained by finite-amplitude effects. Because of the considerable difficulties in performing stability experiments, these experiments should be repeated with great care to see if the earlier measurements can be confirmed. In doing that, all experimental conditions should be documented in greater detail than before to facilitate comparison with theory or numerical simulations.

3.4. *Wavenumbers of the disturbance waves and comparison with linear stability theory*

The effect of the non-parallel mean flow on the wavenumber can be investigated by a thorough comparison of the results obtained from the Navier–Stokes calculations with those obtained from the linear (parallel) stability theory. The wavenumber α_r (dimensionless with the reference length L) is calculated from the Navier–Stokes solution by using the phases that result from a Fourier analysis of the instantaneous disturbances (see (3.2)).

The relationship for calculating the wavenumbers α_r are

$$\left.\begin{aligned} \alpha_{r_u} &= \frac{\partial \Theta_{u_1}(x,y)}{\partial x} \quad \text{for } u', \\ \alpha_{r_v} &= \frac{\partial \Theta_{v_1}(x,y)}{\partial x} \quad \text{for } v', \\ \alpha_{r_v} &= \frac{\partial \Theta_{\omega_1}(x,y)}{\partial x} \quad \text{for } \omega'. \end{aligned}\right\} \tag{3.5}$$

Therefore, different wavenumbers, α_{r_u}, α_{r_v}, α_{r_ω} can be calculated depending on whether they are obtained from the u', v' or ω' disturbances, respectively. In addition these wavenumbers are dependent on x and y while standard parallel theory would of course only yield a dependency on x, $\alpha_r = \alpha_r(x)$.

For calculation cases 1 and 4 the wavenumbers α_r as obtained from the u', v' and ω' disturbances are shown in figure 20. For comparison, the curves from linear-stability theory are given also. The Navier–Stokes results are shown for two different distances from the wall. It is obvious that the wavenumber is strongly dependent on the distance from the wall. In particular, closer to the wall the wavenumber relations with respect to x are somewhat different depending on whether they are obtained from the u', v' or ω' disturbance field. On the other hand, further away from the wall, the wavenumber relations are essentially the same, independent of whether they are determined from u' or v'. This is consistent with our earlier observation in connection with the growth rates α_i, namely that non-parallel effects are strongest close to the wall and that their influence on the different variables becomes negligible far away from the wall.

4. Conclusions

The results from our Navier–Stokes calculations clearly indicate that the concept by Bouthier of a partial and total instability is not a reasonable one, even if, as he suggested, the instability criterion is based on the local kinetic energy and following

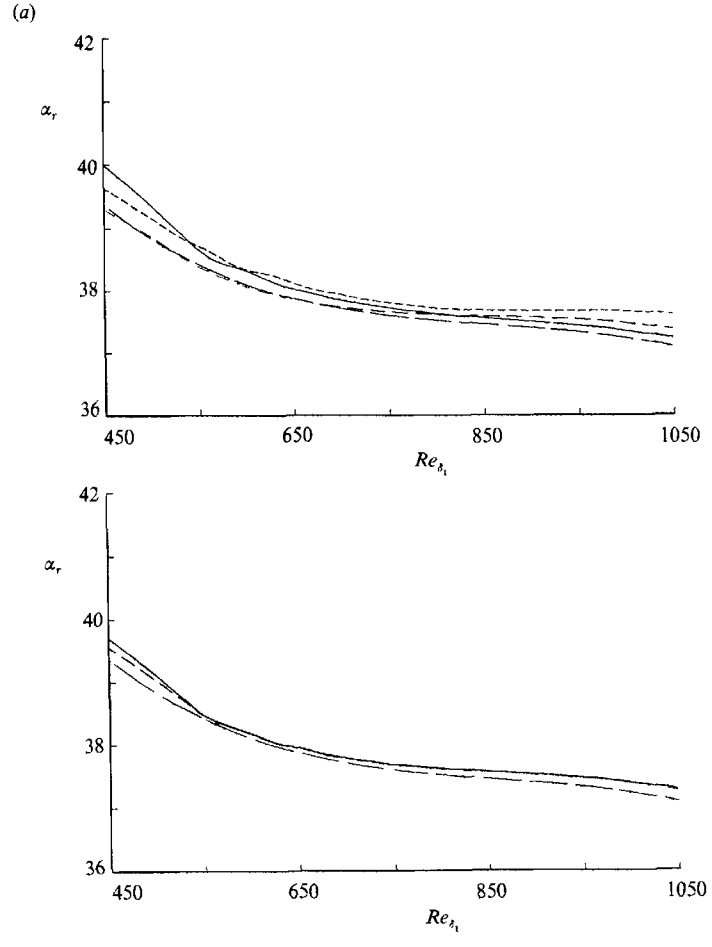

FIGURE 20(a). For caption see facing page.

the disturbance development at constant η. According to Bouthier's definition, regions of total instability for a given frequency are those where disturbances are amplified at all distances η from the wall. For regions of partial instability, amplification occurs at least one distance η from the wall.

With this concept of partial and total instability Bouthier claims good agreement of his results with experimental measurements (for the neutral curves). However, our results and results by Van Stijn & Van de Vooren have shown (Van Stijn & Van de Vooren, figure 2) that for larger η-values ($\eta > 17$, for $F = 1.4$), based on his criterion, disturbances would be damped at all frequencies and therefore no total instability would exist. This fact escaped Bouthier's attention because he limited his calculation to $\eta = 4$. If he had considered values $\eta > 4$ he would have arrived at the same conclusion.

The comparison of Bouthier's results with experiments is meaningless for another reason. The experimental neutral points by Schubauer & Skramstad, Ross *et al.*, and Kachanov *et al.* were obtained for the u'-disturbances (following at constant y, constant η or the maximum of u') and not for the local kinetic energy. As can be

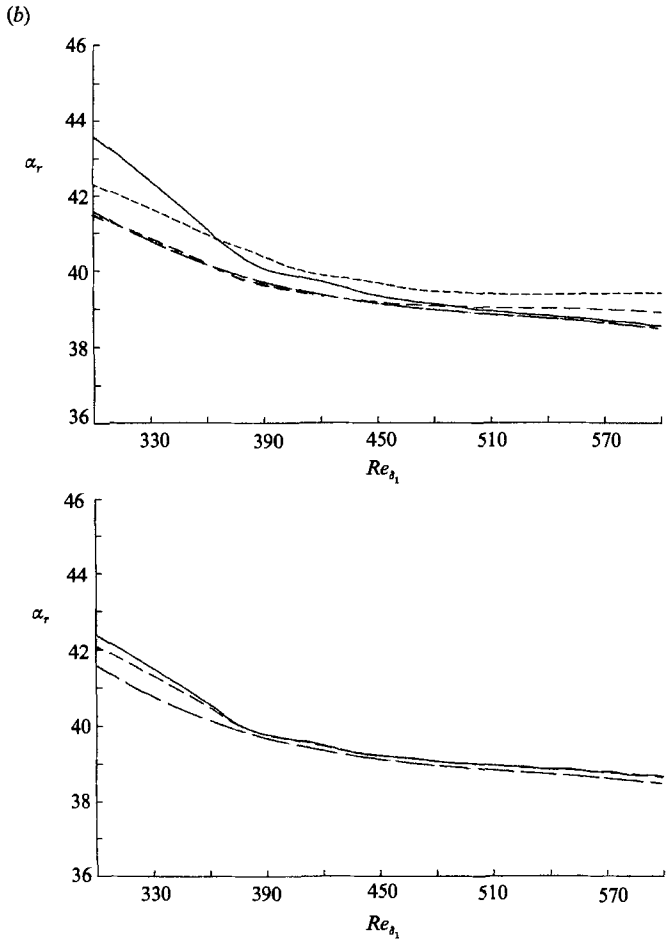

FIGURE 20. Wavenumber α_r versus Re_{δ_1} for two y locations y_1 and y_2 as determined from u', v' and ω'. (*a*) case 1, $F = 1.4 \times 10^{-4}$, $y_1 = 2.51$, $y_2 = 10.0$; (*b*) case 4, $F = 3.0 \times 10^{-4}$, $y_1 = 1.66$, $y_2 = 6.64$. Navier–Stokes solution: ——; α_{ru}; – – –, α_{rv}; - - -, $\alpha_{r\omega}$. ————, parallel theory.

observed from comparison of figures 13 and 14 the location of the neutral points is significantly different if the local kinetic energy is considered instead of the u'-disturbance itself.

This wide variation of the location of the neutral points for the u'-disturbance when following different trajectories η = constant or y = constant as obtained from our Navier–Stokes calculations explains the often contradictory results obtained from experimental stability investigations: by just following the disturbance at different η or y = constant the neutral locations may be shifted by as much as 200 Re_{δ_1}. The most extreme variations of the neutral locations are experienced near the 180° phase-shift locations. Therefore, any comparisons of theory with experiments for y or η close to the 180° phase-shift location are suspect.

The close agreement of the neutral curve given by Saric & Nayfeh (1975) cannot be due to non-parallel effects. Rather the close agreement was fortuitous and was caused by an error in the analysis. With a correction of their analysis their results essentially agree with those of Gaster (1974) when identical criteria are considered (Saric, private communication).

The major non-parallel effects can be summarized as follows:

(*a*) There is no universal amplification rate α_i as in the parallel theory. Rather, growth rates depend strongly on the criteria used (variables, distances from wall, etc.).

(*b*) Depending on the underlying criteria, the neutral location and therefore the size of the unstable region can vary considerably.

(*c*) There is no universal wavenumber α_r as in parallel theory. As for the growth rate α_i, the wavenumber α_r is strongly dependent on the criteria used.

(*d*) The non-parallel effects are strongest closer to the wall (inside the boundary layer) and decrease with increasing distance from the wall.

However, non-parallel effects do not:

(*a*) influence the amplitude and phase distributions as obtained from parallel linear-stability theory,

(*b*) fully account for the discrepancy between experimental and theoretical (parallel theory) neutral curves.

The detailed and accurate Navier–Stokes calculations discussed in this paper have shown that the amplitude and phase distributions with respect to y practically coincide with those obtained from the eigenfunctions of linear (parallel) stability theory (spatial formulation). Therefore, the use of the amplitude distributions of the parallel theory as a first approximation for an extension of the theory to include non-parallel effects is well justified (for example Bouthier 1972, 1973; Gaster 1974; Saric & Nayfeh 1975, 1977; Van Stijn & Van de Vooren 1983; Bridges & Morris 1987).

The financial support of this research by the Deutsche Forschungsgemeinschaft under contracts Fa 117/2-1 and Fa 117/2-2 is gratefully acknowledged.

REFERENCES

Barry, M. D. J. & Ross, M. A. S. 1970 *J. Fluid Mech.* **43**, 813.

Bestek, H. 1980 Numerische Untersuchungen zur nichtlinearen räumlichen Störungsanfachung in der ebenen Poiseuille-Strömung. Dissertation. Universität Stuttgart.

Bouthier, M. 1972 *Méc.* **11**, 599.

Bouthier, M. 1973 *J. Méc.* **12**, 75.

Bridges, T. J. & Morris, P. J. 1987 *Phys. Fluids* **30**, 3351.

Fasel, H. 1974 Untersuchungen zum Problem des Grenzschichtumschlages durch numerische Integration der Navier–Stockes Gleichungen. Dissertation, Universität Stuttgart.

Fasel, H. 1976 *J. Fluid Mech.* **78**, 355.

Fasel, H. 1979 Numerische Simulation inkompressibler viskoser Strömungen. Habilitationsschrift. Universität Stuttgart.

Gaster, M. 1962 *J. Fluid Mech.* **14**, 222.

Gaster, M. 1965 *Prog. Aerospace Sci.* **6**, 2510.

Gaster, M. 1974 *J. Fluid Mech.* **66**, 465.

Heisenberg, W. 1924 *Annln Phys.* **74**, 577.

Hoeptner, C. P. 1981 Nichtlineare Behandlung von Tollmien–Schlichting-Wellen durch numerische Simulation. Diplomarbeit. Universität Stuttgart.

Jordinson, R. 1970 *J. Fluid Mech.* **43**, 801.

Kachanov, Yu. S., Kozlov, V. V. & Levchenko, V. Y. 1979 *Fluid Mech. Sov. Res.* **8**, 152.

Konzelmann, U. 1983 Nichtlineare Wellenausbreitung in einer Grentschichtströmung (numerische Untersuchung). Diplomarbeit. Universität Stuttgart.

Konzelmann, U., Rist, U. & Fasel, H. 1987 *Z. angew. Math. Mech.* **67**, T298.

KÜMMERER, H. 1973 Numerische Untersuchungen zur Stabilität ebener laminarer Grenzschichtströmungen. Dissertation. Universität Stuttgart.

LANCHON, H. & ECKHAUS, W. 1964 *J. Méc.* **3**, 445.

LIEPMANN, H. W., BROWN, G. L. & NOSENCHUCK, D. M. 1982 *J. Fluid Mech.* **118**, 187.

LIEPMANN, H. W. & NOSENCHUCK, D. M. 1982 *J. Fluid Mech.* **118**, 201.

LING, C. H. & REYNOLDS, W. C. 1973 *J. Fluid Mech.* **59**, 571.

ROACHE, P. J. 1982 *Computational Fluid Dynamics.* Hermosa, Albuquerque.

ROSS, J. A., BARNES, F. H., BURNS, J. G. & ROSS, M. A. S. 1970 *J. Fluid Mech.* **43**, 819.

SARIC, W. S. & NAYFEH, A. H. 1975 *Phys. Fluids* **18**, 945.

SARIC, W. S. & NAYFEH, A. H. 1977 *AGARD Conf. Proc.* **224**, 6.1.

SCHLICHTING, H. 1933 *Z. angew. Math. Mech.* **13**, 171.

SCHUBAUER, G. B. & SKRAMSTAD, H. K. 1947 *J. Aeronaut. Sci.* **14**, 69.

SMITH, A. M. O. & GAMBERONI, N. 1956 *Douglas Aircraft Co. Rep.* ES 26388, El Segundo, California.

SMITH, F. T. 1979 *Proc. R. Soc. Lond.* A **366**, 91.

TOLLMIEN, W. 1929 *Nachr. Ges. Wiss. Göttingen, Math. Phys. Klasse*, p. 21.

VAN INGEN, J. L. 1956 *Univ. of Technology, Dept of Aero. Engng Rep.* UTH-74, Delft.

VAN STIJN, TH. L. & VAN DE VOOREN, A. I. 1983 *Computers Fluids* **10**, 223.

VOLODIN, A. G. 1973 *Izv. Sib. Otd. Akad. Nauk SSSR* **2**, 13.